

Prevalent and Dynamic Binding of the Cell Cycle Checkpoint Kinase Rad53 to Gene Promoters

Yi-Jun Sheu, Risa Karakida Kawaguchi, Jesse Gillis and Bruce Stillman¹

Cold Spring Harbor Laboratory, 1 Bungtown Road, Cold Spring Harbor, NY 11724, USA

¹Correspondence: Bruce Stillman stillman@cshl.edu

Key words: Origins of DNA replication, Transcription start sites, Gene promoters, Checkpoint Kinase, Rad53, Mrc1, DNA damage response, Stress Response

Abstract

Replication of the genome must be coordinated with gene transcription and cellular metabolism. These processes are controlled in part by the Rad53 (CHEK2 in mammals) checkpoint kinase and the Mrc1 replisome component, especially following replication stress in the presence of limiting deoxyribonucleotides. We examined cell cycle regulated, genome-wide binding of Rad53 to chromatin. The kinase bound to sites of active DNA replication initiation and fork progression, but unexpectedly to the promoters of numerous genes (>20% of all genes) involved in many cellular functions. At some genes, Rad53 promoter binding correlated with changes in gene expression. Rad53 promoter binding to certain genes is influenced by sequence-specific transcription factors and less by checkpoint signaling. In checkpoint mutants, untimely activation of late-replicating origins reduces the transcription of nearby genes, with concomitant localization of Rad53 to their gene bodies. We suggest that the Rad53 checkpoint kinase coordinates genome-wide replication and transcription under stress conditions.

30 Introduction

31
32 Eukaryotic cells initiate DNA synthesis in a temporally controlled manner from multiple replication
33 origins to ensure efficient duplication of the genome (Bell and Labib, 2016; Renard-Guillet et al.,
34 2014). During the course of replication, replisomes have to deal with both endogenous and
35 exogenous stresses that can cause stalling of replication forks. The same DNA template is also
36 transcribed, potentially creating conflicts between replication and transcription that can lead to
37 detrimental effects on genome stability and cell viability (Hamperl and Cimprich, 2016).

38
39 To maintain genome stability during S-phase, the budding yeast *S. cerevisiae* activates a DNA
40 replication checkpoint (DRC) in response to replication stress via the sensor kinase Mec1 (the
41 mammalian ATM/ATR), the replication fork protein Mrc1 (Claspin in mammals) and other fork
42 proteins (Lanz et al., 2019; Osborn and Elledge, 2003; Pardo et al., 2017; Paulovich and Hartwell,
43 1995; Saldivar et al., 2017). A second DNA damage checkpoint (DDC) mediated by Rad9 (TP53BP1
44 in mammals) responds to double strand DNA breaks. Both branches converge on the effector kinase
45 Rad53 (CHEK2 in mammals) which triggers a wide range of downstream events, including stopping
46 cell cycle progression, preventing late origin firing, activating the DNA repair and elevating synthesis
47 of deoxyribonucleoside triphosphates (dNTP). The signaling also promotes widespread changes in
48 gene expression (Jaehnig et al., 2013; Pardo et al., 2017).

49
50 Unlike most of the checkpoint genes, both Mec1 and Rad53 kinases are essential for cell viability in
51 unperturbed cells that can be partly explained by their role in regulating dNTP pools (Desany et al.,
52 1998; Forey et al., 2020; Zhao et al., 2000). However, it is important to note that kinase null mutants
53 are extremely sick and sensitive to various type of exogenous stress. Under the bypass conditions in
54 cells without Sml1, the inhibitor of ribonucleotide reductase (RNR), cells lacking Rad53 exhibit a
55 more severe defect than cells lacking Mec1, implying that Rad53 has activities beyond checkpoint
56 signaling. Consistent with this suggestion, the kinase deficient mutant *rad53^{K227A}* lacks checkpoint
57 function but retains growth-associated activity (Gunjan and Verreault, 2003; Hoch et al., 2013;
58 Holzen and Sclafani, 2010; Pelliccioli et al., 1999).

59
60 Rad53 is central to the transcriptional response to DNA damage, including the Dun1 protein kinase
61 acting downstream of Rad53 to phosphorylate and inactivate the transcriptional repressor Rfx1/Crt1
62 and thereby up-regulate target genes (Huang et al., 1998), such as *RNR2*, *RNR3*, and *RNR4*, all
63 encoding subunits of RNR. However, the induced expression of *RNR1*, which encodes the major
64 isoform of the RNR large subunit, is not controlled by the Rfx1 repressor, but by Ixr1 binding to the
65 *RNR1* promoter upon genotoxic stress. This Ixr1-dependent regulation of *RNR1* is independent of
66 Dun1 but requires Rad53 (Tsaponina et al., 2011). Another Rad53-dependent, Dun1-independent
67 regulation of *RNR1* involves phosphorylation-dependent dissociation of Nrm1 from MBF (Travesa et
68 al., 2012).

69
70 In addition to upregulating the dNTP pools, defects in cells lacking Rad53 can be suppressed by
71 manipulating factors functioning in transcription regulation, cell wall maintenance, proteolysis and
72 cell cycle control (Desany et al., 1998; Manfrini et al., 2012). Moreover, Rad53 kinase targets and
73 interaction partners found in biochemical and proteomic studies suggests that the kinase is pleiotropic
74 (Gunjan and Verreault, 2003; Jaehnig et al., 2013; Lao et al., 2018; Smolka et al., 2007, 2006).

75

76 In this study, while investigating of the response of yeast cells to replication stresses caused by
77 depletion of dNTPs, we found that Rad53 not only binds to sites of DNA synthesis, but it localized to
78 more than 20% of gene promoters in the *S. cerevisiae* genome, suggesting a global role in
79 coordinating stress responses. Furthermore, we provide evidence that untimely activation of
80 replication from late origins can negatively affect transcription activity of nearby genes.

81

82 **Results**

83

84 **Initiation, elongation and recovery of DNA replication in checkpoint mutants**

85

86 DNA replication in the presence of low dNTP levels was examined by releasing G1-phase cells for
87 either 45 (HU45) or 90 (HU90) minutes into media containing hydroxyurea (HU), coupled with
88 labeling DNA synthesis with 5-ethynyl-2'-deoxyuridine (EdU) (Sheu et al., 2016, 2014). The purified
89 EdU-DNA was subjected to high-throughput DNA sequencing and the reads were mapped to the
90 genome, yielding replication profiles for wild-type (WT) and three DNA damage checkpoint mutants,
91 *rad53^{K227A}* (a kinase-deficient version of Rad53), *mrc1Δ* (null for *Mrc1* mediator of the DRC branch)
92 and *rad9Δ* (null for *Rad9* mediator of DDC branch).

93

94 In WT cells, DNA synthesis occurred only from early origins because of the activated DRC
95 checkpoint, which inhibits late origin firing (Figure 1a, [HU90] and Figure 1-figure supplement 1a
96 [HU45 and HU90])^{5,6}. As expected DNA synthesis was readily detected from late origins (red
97 arrows) in the kinase-deficient *rad53^{K227A}* and *mrc1Δ* mutants. In contrast, the *rad9Δ* mutant profile
98 appeared identical to that of WT (Figure 1a). Thus, the DRC branch (*Mrc1*), but not the DDC branch
99 (*Rad9*), represses late origin firing in response to this replication stress.

100

101 Among the 829 active or potential origins of DNA replication (Siow et al., 2012), 256 origins are
102 active in WT cells and 521 origins are active in the *rad53^{K227A}* and *mrc1Δ* mutants, specifying “early”
103 (E) and “late” (L) firing origins, respectively. The remaining 308 were therefore inactive (I) under
104 these conditions. The EdU peak signals in each mutant for these origin categories shows that the
105 *rad53^{K227A}* mutant favored late origins over early origins (Figure 1b), which was particularly
106 prominent in heterochromatic regions on chromosome III, such as *HMR*, *HML* and telomere-proximal
107 regions harboring very late firing origins (Figure 1-figure supplement 1b). This pattern is not seen in
108 the *mrc1Δ*, suggesting that it is due to loss of Rad53 kinase activity but not DRC signaling.

109

110 Rad53 is required for stability of DNA stalled replication forks (Bacal et al., 2018; Kumar and
111 Huberman, 2008; Lopes et al., 2001; Seiler et al., 2007; Tercero et al., 2003), which was confirmed
112 by labelling DNA synthesis during recovery from HU-induced replication stress. Cells that
113 progressed from G1- into S-phase in HU for 45 min. were released from the HU block and DNA
114 synthesis labeled with EdU during an additional 25 min (HU→S25) or were continued in HU for
115 another 45 min. and labeled with EdU (HU→HU45) (Figure 1c). In *WT* cells, DNA synthesis during
116 recovery from HU continued from the stalled replication forks (Figure 1d). For very efficient early
117 origins, such as *ARS305*, *ARS306* and *ARS307* (Figure 1d, black arrows), little new synthesis
118 occurred at origins during the recovery, suggesting efficient initiation at these origins. In contrast, for
119 moderately early origins, such as *ARS309* and *ARS315* (Figure 1d, brown arrows), DNA synthesis
120 occurs at both the origin and recovered forks in the cell population. DNA synthesis from late origins

121 is not detectable (Figure 1d, red arrows). Thus, in *WT*, DNA synthesis during recovery from
122 replication stress continued mainly from already activated replisomes that had progressed away from
123 origins. If the replication stress persisted, DNA synthesis continued slowly only from existing
124 replisomes (Figure 1d).

125
126 In the recovering *mrc1Δ* mutant, DNA synthesis continued from stalled replisomes, albeit slowly, but
127 unlike *WT*, new initiation at efficient early origins, such as *ARS305*, *ARS306* and *ARS307* was also
128 detected (Figure 1d), suggesting that Mrc1 is important for efficient initiation at early origins in
129 addition to its established role in stimulating fork progression (Osborn and Elledge, 2003; Tourrière
130 et al., 2005; Yeeles et al., 2016). During recovery from stress, the *rad53^{K227A}* mutant failed to restart
131 DNA synthesis at most stalled forks, except for the replicons in the heterochromatic regions, where
132 new initiation was also detected (Figure 1d). Thus, the replication fork collapse was more severe in
133 the absence of Rad53 kinase compared to the absence of checkpoint signaling in the *mrc1Δ* mutant.
134

135 **Rad53 is recruited to sites of DNA synthesis independent of checkpoint** 136 **signaling**

137
138 To investigate the status of replisomes, chromatin immunoprecipitation and deep sequencing (ChIP-
139 seq) was employed to follow localization of Cdc45, which is associated with activated helicases at the
140 replisomes. G1 arrested cells and cells released for 45 and 90 min. in HU were processed for ChIP-
141 seq analysis (Behrouzi et al., 2016).

142
143 Using either normalized read counts or a heatmap analysis around active origins that are ranked in
144 order of DNA replication timing²⁸, Cdc45 in *WT* cells was found moving only from early origins,
145 (Figure 2a and 2b; early origins in top panel and late origins in bottom panel). In contrast, Cdc45 is
146 present at both early and late origins in both *rad53^{K227A}* and *mrc1Δ* mutants, with slower progression
147 in the *mrc1Δ* mutant (Figure 2b; Figure 2- figure supplement 1a), consistent with its role in
148 progression at replication forks (Tourrière et al., 2005; Yeeles et al., 2016). Cdc45 in the *rad53^{K227A}*
149 mutant emanating from late origins continued to move from HU45 to HU90, whereas at the early
150 origins Cdc45 signal did not move further away for origins (Figure 2b). Since Cdc45 can recruit
151 Rad53 to restrict CMG helicase activity (Can et al., 2018; Devbhandari and Remus, 2020), the limited
152 Cdc45 signal at early origins here suggests that, in the absence of active Rad53 kinase, replisomes
153 departed from origins but disintegrated. The persistent signal at origins in HU90 is consistent with
154 firing at early origins in those cells that had not initiated DNA replication during the HU block.

155
156 Phosphorylation of histone H2A at serine 129 (S129; γ -H2A) by the sensor kinase Mec1 is an
157 indication of checkpoint activation. γ -H2A ChIP-seq monitors the genome distribution of checkpoint
158 activation under HU stress (Figure 2c and d; Figure 2 – figure supplement 1b). In *WT* cells, γ -H2A
159 signals are particularly high around the earliest firing origins in HU45 and HU90, suggesting that
160 stress signals emit mostly from early origins. In the *rad53^{K227A}* and *mrc1Δ* mutants, γ -H2A is found at
161 both early and late origins, however, in the *rad53^{K227A}* mutant, the signal at early firing origins
162 reduces with time, suggesting that Rad53 kinase activity is needed to maintain stress signaling by
163 Mec1 at early origins. In contrast, the Mrc1 is not strictly required to induce or maintain γ -H2A.
164

165 Interestingly, γ -H2A is observed at genomic regions surrounding the very late origins in G1-phase in
166 both WT and mutants (Figure 2d and Figure 2 – figure supplement 1b). It is possible that these γ -
167 H2A signals reflect a low level of ssDNA gaps at these late-replicating regions that was tolerated and
168 carried over from the previous cell cycle, similar to unrepaired post-replication gaps resulting from
169 low level of UV irradiation in *S. pombe* G2-phase (Callegari and Kelly, 2006).

170
171 Rad53 kinase detected by ChIP-seq at genome sites in WT cells largely follows the progression of
172 replication forks (Figure 2e and f; Figure 2 – figure supplement 1c). Rad53 is also detected at late
173 origins in both checkpoint mutants, but dispersed at late times in the *rad53*^{K227A} mutant. The
174 spreading of Rad53 signal in the *mrc1* Δ mutant is more restricted, consistent with slower replication
175 fork progression. Surprisingly, Rad53 binding to replication forks does not require the Mrc1,
176 suggesting checkpoint-independent recruitment of Rad53 to sites of DNA synthesis.

177

178 **Rad53 binds to promoters of genes involved in multiple cellular processes**

179

180 Unexpectedly, we noticed many Rad53 peaks even in G1 arrested cells (Figure 2e) and many of these
181 peaks localized upstream of transcription start sites (TSS) or promoters (Figure 3). In *WT*, some peak
182 signals change as cells progress from G1-phase into HU arrested S-phase. For example, Rad53 at the
183 *RNR1* promoter increases from G1 to HU45 and HU90 (Figure 3a and b). A similar pattern occurs at
184 the *RNR3* promoter. The Rad53 signal at promoters are present in both *rad53*^{K227A} and *mrc1* Δ mutants
185 (Figure 3a). Rad53 binding to promoters also occurs in the *sml1* null mutant (*sml1* Δ) and the *mec1*
186 null mutant (*mec1* Δ *sml1* Δ), but is absent in *rad53* null (*rad53* Δ *sml1* Δ), demonstrating antibody
187 specificity (Figure 3b and Figure 3 – figure supplement 1a). Thus, both the sensor kinase Mec1 and
188 Mrc1 are not required for the recruitment of Rad53 to these sites.

189

190 Whole genome analysis shows that ~90% of the Rad53 peaks are either upstream of or overlap the
191 TSS (Figure 3 – figure supplement 1b). Rad53 promoter binding is temporally dynamic in a subset of
192 genes, suggesting regulation by cell cycle progression or DNA replication stress. Heatmaps of the
193 Rad53 signals at 2 kb intervals centered on all transcription start sites (TSS) show a global trend of
194 increasing Rad53 binding as cells progress from G1-phase into HU45 or HU90 (Figure 3c),
195 concomitant with increased levels of Rad53 protein in cells treated with HU (Figure 3 – figure
196 supplement 2a). The increase parallels entry into S-phase, as measured by Orc6 phosphorylation,
197 destruction of Sml1 and histone H2A phosphorylation (Figure 3 – figure supplement 2a-c).
198 Additional genes show increased Rad53 binding as cells progress from G1- into S-phase (Figure 4a,
199 upper panels), but at other promoters Rad53 binding decreases during the same time course (Figure
200 4a, lower panels). However, at most genes Rad53 remains constant.

201

202 In this study, two sets of duplicate Rad53 ChIP-Seq experiments were performed in WT, *rad53*^{K227A}
203 and *mrc1* Δ mutants (CP set), and based on the type of genes that bind Rad53, in transcription factor
204 mutants *ixr1* Δ , *swi4* Δ , *swi6* Δ and WT (TP set). Residual analysis in WT identified the top
205 differentially binding (DB) genes (Figure 4b, Figure 4c for CP and TP sets; orange dots). Among the
206 top 1000 DBs from each set, 435 genes were identified in both (Figure 4b, 435 Top DB overlap).
207 Overall, during the G1- to S-phase transition (HU45), there are more genes with increased Rad53
208 promoter binding than those with decreased binding. Many of these genes encode proteins involved
209 in cell cycle progression (e.g., cyclins and regulators of DNA replication) and cell growth (e. g., cell
210 wall maintenance and mating response).

211
212 In the *rad53^{K227A}* mutant, the increase in Rad53 promoter binding is transient and generally weaker,
213 consistent with lower protein levels (Figure 3c). In the *mrc1Δ* mutant, the binding at the *RNR1*
214 promoter is reduced compared to WT, despite an increase Rad53 protein (Figure 3a, Figure 3 – figure
215 supplement 2a). In contrast, the increase in Rad53 binding at the *PCL1* promoter appears to be less
216 affected by the checkpoint mutations (Figure 3a). Thus, the DRC checkpoint only affects differential
217 binding of Rad53 to a subset of promoters. At other promoters, cell cycle progression or response to
218 mating pheromone due to treatment and removal of α -factor may contribute to differential Rad53
219 promoter binding.

220
221 Visual inspection of the ChIP-Seq peaks suggested that Rad53 bound to numerous gene promoters
222 and TSSs throughout the genome. Rad53 ChIP-Seq was compared to a previous ChIP-Seq data set of
223 the sequence-specific transcription factor Swi6, part of SBF and MBF that control cell-cycle
224 regulated genes (Breedon, 2003). The Gini indices computed for Swi6 and two of our Rad53
225 replicates are 0.763, 0.2918, and 0.2982, respectively, calculated from Lorenz curves (Figure 3d).
226 Rad53 has a higher coverage for many promoters while Swi6, as expected, shows substantially high
227 coverage only for a limited number of promoters.

228

229 **The relationship between Rad53 promoter binding and gene expression**

230

231 The relationship between Rad53 promoter recruitment was compared to gene expression from RNA-
232 seq analysis using the same conditions. RNA-seq replicates from 4 strains (*WT*, *rad9Δ*, *rad53^{K227A}*
233 and *mrc1Δ*), each with 3 stages (G1, HU45 and HU90) were analyzed using rank data analysis
234 (Figure 5a). The expression profiles in G1 are very similar among all strains. In HU, however, two
235 groups are evident; *rad9Δ* is like WT since Rad9 has no role in the DRC checkpoint branch. In
236 contrast, *rad53^{K227A}* and *mrc1Δ* cluster together in both HU45 and HU90, consistent with Rad53 and
237 Mrc1 functioning together in the response to HU stress.

238

239 In the hierarchical clustering, cell cycle stage contributes more to similarities than the genotype
240 (Figure 5a). Pair-wise comparison of G1 to HU45 in WT and *rad9Δ* cells shows that ~2300 genes
241 exhibited significant expression changes (differentially expressed genes; DEGs; Figure 5b). The
242 number of DEGs increases further to ~3000 when comparing G1 to HU90. In both *rad53^{K227A}* and
243 *mrc1Δ* mutants, ~2500 DEGs are detected from G1 to HU45, which increases to >3400 in G1 to
244 HU90. The response to cell cycle stage is largely equally distributed between up and down regulation.
245 A WT and *rad9Δ* comparison shows only 5 DEGs, demonstrating that Rad9 does not contribute to
246 gene expression changes under HU stress.

247

248 The overall heatmap signal of Rad53 upstream of TSSs is higher in the significant DEGs than in the
249 insignificant DEGs, suggesting that Rad53 may play a role in control of gene expression (Figure 5c
250 and Figure 5 – figure supplement 1). Gene co-expression analysis of the RNA-seq data yields ten co-
251 expression clusters of DEGs in WT (G1→HU45) (Figure 6a and Figure 6 – figure supplement 1).
252 Specific, dynamic Rad53 binding at promoter regions occurs in most clusters (Figure 6b), with GO
253 functions including cell cycle regulation, mating response, proteolysis, transport, oxidation-reduction
254 process and organic acid metabolism (Figure 6a).

255

256 Within the 435 Top DB overlapping genes (Figure 4b), 236 show significant expression changes.
257 Plots of Rad53 binding changes against gene expression changes of these 236 genes show a positive
258 correlation between Rad53 binding change and gene expression change (Figure 6c, left panel).
259 Among this group, 51 out of 54 genes with decreased Rad53 signal are down-regulated in mRNA
260 levels. Genes with increased Rad53 signals are partitioned between up-regulation and down-
261 regulation (108 and 74, respectively). Further break down of the 236 gene group into co-expression
262 clusters of the DEGs in WT (G1→HU45) revealed that genes in clusters 1 and 7 exhibit the strongest
263 correlation between Rad53 binding and gene expression changes (Figure 6c). Thus, specific subsets
264 of DEGs in the shift from G1→HU exhibit correlations between a change in gene expression and
265 Rad53 promoter binding.

267 **Checkpoint mutants cause down-regulation of gene expression near** 268 **promiscuously active late origins**

269
270 Upon inspection of Rad53 heatmaps around TSSs, we noticed that in several co-expression clusters
271 from the DEGs in the HU45 (*mrc1Δ* vs *WT*) comparison (Figure 7a), down-regulated genes tend to
272 have a strong Rad53 signal not only upstream of the TSS, but a broad signal within gene bodies
273 (Figure 7b). This pattern is prominent in the *mrc1Δ* mutant at HU45 and further intensifies in HU90.
274 The gene body localization is also found transiently in *rad53^{K227A}* cells (Figure 7 – figure supplement
275 1). Such a gene body signal is not as prevalent in the WT HU45 and HU90 samples. Since Rad53 is
276 also recruited to active origins and moves with the replication fork, we suspected these gene body
277 signals in the checkpoint mutants may be caused by the promiscuous activation of near-by origins
278 that are normally inactive in WT, creating conflicts between DNA replication and gene transcription.
279 The transient nature of the Rad53 localization at gene body in this group of genes in the *rad53^{K227A}*
280 mutant is also consistent with the transient signal pattern at these late origins (Figure 2f, bottom
281 panel). Thus, we investigated the relationship between these genes and their closest replication
282 origins.

283
284 The distance of replication origins to the nearest TSS, the relative orientation of the gene to the origin
285 (head-on or co-directional) and the origin type (early, late or inactive; Figure 1b) was determined and
286 correlated with the DEG clusters (Figure 7c). Overall, most of the down regulated genes in cluster 1
287 of this group are situated very close to active origins (< 2 kb between origin center and TSS, light
288 purple marks and <1 kb, dark purple marks). Interestingly, the pattern of origin to promoter distance
289 marks largely mirrored the pattern of the Rad53 ChIP signal within the gene bodies (Figure 7b and
290 7c). This correlation pattern is not found in the WT ChIP heatmap. Within the DEG group, genes
291 situated 5 kb or more away from closest active origins are similarly distributed between up regulation
292 and down regulation of gene expression (Figure 7d, left panels). However, for those genes that are
293 closer to an active origin, the bias to be down regulated gene increases. For those that gene situated
294 less than 1 kb away from active origins, more than 80% are down-regulated genes.

295
296 The DEGs in HU45 (*mrc1Δ* vs *WT*) that are more than 5 kb away from active origins are also
297 similarly distributed between up and down regulation (Figure 7d, middle panels). More down
298 regulated genes are found when the nearby origins are active. The bias is even stronger for genes that
299 are close to late origins, which become active in HU when Mrc1 is absent. Because late origins and
300 intermediate early origins are more active in the *mrc1Δ* mutant, it is possible that nearby gene
301 expression is negatively affected by active DNA synthesis. Furthermore, the bias toward the down

302 regulation is even stronger (>80%) when the nearby origin is in a head-on orientation towards the
303 gene (Figure 7d, right panels). Similarly, a bias exists toward down regulation of DEGs from HU45
304 (*rad53^{K227A}* vs *WT*) that are close to active origins (Figure 7 – figure supplement 1). The tendency to
305 find a high Rad53 signal at gene bodies in the *mrc1Δ* and *rad53^{K227A}* mutants also occurred in the
306 down-regulated DEGs in *mrc1Δ* (G1→HU45) (Figure 5 – figure supplement 1c), likely caused by
307 the same proximal origins. Thus, the untimely activation of replication origins in the checkpoint
308 mutants affects gene expression and Rad53 binding to gene bodies.

309 310 **Rad53 binding changes coincide with the changes in gene expression for targets of** 311 **cell cycle regulators SBF, MBF and mating response regulator Ste12**

312
313 The DEGs in WT (G1→HU45) were associated with co-expression clusters that showed a strong
314 correlation between Rad53 binding and gene expression (Figure 6c, clusters 1 and 7). They contain
315 genes that encode targets of SBF and MBF, key transcription factor complexes comprised of a shared
316 regulatory subunit, Swi6 and the DNA-binding subunits Swi4 and Mbp1, respectively (Breedon,
317 2003). Their target genes include multiple G1- and S-phase cyclin genes, such as *PCL1*, *CLN1*,
318 *CLN2*, *CLB5*, *CLB6*. Evidence suggests that SBF and MBF are directly regulated by Rad53 kinase
319 (Oliveira et al., 2012; Sidorova and Breedon, 2003; Travesa et al., 2012) and Rad53 may regulate
320 expression of targets of Msn4, Swi6, Swi4, and Mbp1 through Dun1-independent mechanisms
321 (Jaehnig et al., 2013). Thus, we analyzed the annotated targets of these transcription factors compiled
322 in the *Saccharomyces* Genome Database (SGD; <https://www.yeastgenome.org>). Among the 81 genes
323 that are candidate targets for both Swi4 and Swi6, 36 genes were found in the 236 significant DEGs
324 in the Top DB overlap (Figures 4b and 6c) with an enrichment of 12.91. Scatter plot comparisons of
325 Rad53 binding and gene expression changes of these 36 genes show a clear positive correlation
326 (Figure 8a, SBF top panel). Combining the data from the checkpoint mutants (Figure 8a, SBF bottom
327 panel and Figure 8 – figure supplement 1a) show that most of these genes have similar levels of
328 differential expression in the *rad9Δ* mutant compared with WT from G1 to HU45, whereas in the
329 *mrc1Δ* and *rad53^{K227A}* mutants exhibit different level of changes. Similar plot patterns were found
330 with 26 out of 65 MBP targets with an enrichment of 11.62 (Figure 8a and Figure 8 – figure
331 supplement 1b), including overlap between the targets of SBF and MBF (19 genes). We also found
332 enrichment for targets of transcription factor Msn4 and patterns of correlation (Figure 8a and Figure 8
333 – figure supplement 1d, Msn4 panels), including 12 out of 22 Msn4 targets that are also SBF targets.

334
335 Many of the genes with decreased Rad53 binding at the promoters are mating response genes
336 (Figures 4b and c). Therefore, the targets of Ste12, a key transcription factor activated by MAPK
337 signaling to activate genes involved in mating or pseudohyphal/invasive growth pathways were
338 investigated. Of 183 potential targets of Ste12 annotated in SGD, 34 are in the 236 significant DEGs
339 in the Top DB overlap (Figures 6c and 8a). All the Ste12 targets that have decreased Rad53 binding
340 are down regulated as cells entered S-phase. Moreover, 20 out of the 34 Ste12 targets in the Top DB
341 group show increased Rad53 binding in HU and 11 of these 20 genes are also targets of SBF. Thus,
342 regulation by SBF appears to be responsible for the correlation between increased Rad53 binding at
343 the promoter and up-regulation of these target genes.

344
345 **SBF plays a major role in the localization of Rad53 to the promoters of its target**
346 **genes under replication stress**

347
348 To determine the contribution of various transcription regulators in recruitment of Rad53 to gene
349 promoters, Rad53 ChIP-seq analysis in *WT*, *ixr1Δ*, *swi4Δ* and *swi6Δ* mutants was performed. In the
350 scatter plot of the Rad53 signal upstream of TSSs in G1 versus HU45 from the *WT* sample, SBF
351 targets in the Top DB (Figure 8b, orange/red diamonds) showed significant deviation from the global
352 trend (blue dots). In *swi4Δ* and *swi6Δ* mutants, the signal for all of these SBF targets collapses
353 towards the global trend (purple and light olive dots, *swi6Δ* and *swi4Δ*, respectively), suggesting that
354 Rad53 signal changes at these genes depends on SBF. In the *ixr1Δ* mutant (green dots), the majority
355 of these SBF targets remain deviated from the global trend in the scatter plot, except for the *RNR1*
356 gene, indicated in the close-up plots (Figure 8b, lower panels), whose position collapsed in all three
357 mutants. Rad53 binding to the *RNR1* promoter is reduced in both SBF mutants, consistent with *RNR1*
358 being a target of SBF and MBF ((Bruin et al., 2006)). Rad53 binding is completely eliminated from
359 the *TOS6* (target of SBF 6) promoter while for *PCL1* and *YOX1*, both targets of SBF, Rad53 binding
360 does not increase in HU. Interestingly, at the promoter of *RNR3*, the paralog of *RNR1*, Rad53 binding
361 in the SBF mutants is low, even though *RNR3* may not be a SBF or MBF target. On the other hand,
362 *ixr1Δ* reduces Rad53 binding to *RNR1* in HU but has no effect on Rad53 recruitment at the *RNR3*
363 promoter (Figure 8c).

364 365 **Discussion**

366
367 Following hydroxyurea induced replication stress, Rad53 was recruited to active origins of DNA
368 replication and to DNA replication forks in a checkpoint independent manner since *mrc1Δ* and
369 *rad53^{K227A}* mutants had little effect on binding. Rad53 is targeted to replisomes by the helicase
370 subunits Cdc45 and Mcm2 where it is activated by Mec1 kinase dependent on Mrc1 at the fork, and
371 stabilizes the replisome (Can et al., 2018; Cobb et al., 2005; Lou et al., 2008; McClure and Diffley,
372 2021; Szyjka et al., 2008). Maintenance of Rad53 at the replication forks requires Rad53 kinase
373 activity but not DRC checkpoint signaling. Since Rad53 kinase can auto-activate itself (Gilbert et al.,
374 2001; Lanz et al., 2019; Pardo et al., 2017; Saldivar et al., 2017), we suggest that either auto-
375 activation or binding to a phosphorylated replisome protein is required for the continued presence of
376 Rad53 at replication forks.

377
378 Checkpoint signaling also prevents replication initiation in late replicating regions of the genome
379 (Hamperl and Cimprich, 2016). However, in the checkpoint mutants, these late origins become active
380 and Rad53 was recruited to the body of origin proximal genes. Concomitantly, gene expression of
381 these genes was reduced, perhaps mediated by recruitment of Rad53. We suggest that the normal
382 temporal order of replication of the genome throughout S-phase has evolved to prevent conflicts
383 between replication and transcription, which is particularly important in a gene dense genome such as
384 *S. cerevisiae*. It is known that late replicating genes are tethered to the nuclear pore complexes in the
385 nuclear periphery and checkpoint signaling, including Rad53 kinase, is required for preventing
386 topological impediments for replication fork progression (Bermejo et al., 2011; Hamperl and
387 Cimprich, 2016). Moreover, during normal replication, Mec1 may locally activate Rad53 to deal with
388 difficult to replicate regions or regions of replication-transcription conflict without triggering full
389 blown checkpoint activation (Bastos de Oliveira et al., 2015). Rad53 kinase inhibits Mrc1 stimulation
390 of the CMG helicase (McClure and Diffley, 2021), consistent with our observation that replication
391 fork progression is limited in the absence of Mrc1 and that replication forks cannot be rescued after
392 DNA damage in *rad53^{K227A}* cells (Forey et al., 2020).

393
394 Unexpectedly we also found Rad53 constitutively bound to > 20% of the gene promoters in the yeast
395 genome, independent of Mrc1 and Rad53 kinase activities. The genes encode proteins with diverse
396 activities, including various aspects of cell cycle, metabolism, protein modification, ion transport, cell
397 wall organization and cell growth. The levels of Rad53 binding to most of these genes did not change
398 during the time course in HU, whereas Rad53 binding increased at promoters for genes such as
399 *RNR1*, *RNR3* and *TOS6*. In contrast, Rad53 levels decreased on the promoters of genes involved in
400 response to mating pheromone as cells exited from α -factor induced G1 arrest into the cell division
401 cycle. The prevalent and dynamic changes in Rad53 promoter-bound levels did not necessarily
402 depend on checkpoint signaling at genes like *PCL1*, but in some cases such as *RNR1*, the increase in
403 Rad53 levels was reduced in checkpoint mutants.

404
405 The conditions employed in this study, cell cycle entry in the presence of hydroxyurea, may
406 determine the nature of the genes that display dynamic binding of Rad53 to gene promoters. It is
407 known that Rad53 phosphorylates transcription factors such as the SBF and MBF subunit Swi6 and
408 the MBF co-repressor Nrm1 (Sidorova and Breeden, 2003; Travesa et al., 2012) and that Ixr1 controls
409 transcription of *RNR1* (Tsaponina et al., 2011). Removal of Swi4, Swi6 or Ixr1 reduced, and in some
410 cases eliminated Rad53 binding to promoters of genes controlled by these transcription factors.
411 Rad53 bound to the Nrm1 promoter, suggesting an additional regulation of cell cycle-dependent
412 transcription control by Rad53. Rad53 also bound to promoters of genes encoding histones H3 and
413 H4, suggesting that in addition to its known role in histone degradation (Gunjan and Verreault, 2003)
414 Rad53 controls histone gene expression. This is consistent with previous findings that Rad53 targets
415 Yta7 (Smolka et al., 2006), which interacts with FACT to regulate histone gene expression and
416 inhibits Spt21^{NPAT}-regulated histone genes expression (Bruhn et al., 2020; Gradolatto et al., 2008). In
417 the absence of Rad53 protein, histone levels become elevated, causing global effects on gene
418 expression (Bruhn et al., 2020; Tsaponina et al., 2011).

419
420 Our data is consistent with the possibility that the Rad53 kinase contributes to the transcriptional
421 regulation as a structural component, as previously suggested for several MAP kinases (Alepez et al.,
422 2001; Kim et al., 2008; Sanz et al., 2018). Like the stress induced kinase Hog1, Rad53 binding to
423 promoters may be dynamic in other stress conditions, which is under investigation. A major
424 unanswered question is how does Rad53 bind to so many diverse promoter sites.

425

426 **Acknowledgements**

427 This research was supported by NIH grants R01GM45436 and R01LM012736 and a gift from the
428 Goldring Family Foundation. The Cold Spring Harbor Laboratory Cancer Center supported core
429 research resources (P30-CA045508). RKK was supported by Uehara Memorial Foundation
430 Postdoctoral Fellowship.

431

432 **Materials and methods**

433

434 **Yeast strains and methods**

435 Yeast strains generated in this study were derived from W303-1a (MATa ade2-1 can1-100 his3-11,15
436 leu2-3,112 trp1-1 ura3-1) and are described in Supplemental Table 1. All the yeast strains used for
437 the whole-genome DNA replication profile analyses have a copy of the BrdU-Inc cassette inserted
438 into the URA3 locus ((Viggiani and Aparicio, 2006)). For G1 arrest of *bar1* Δ strains, exponentially

439 growing yeast cells ($\sim 10^7$ cell/mL) in YPD were synchronized in G1 with 25 ng/mL of α -factor for
440 150 min at 30°C. For G1 arrest of *BARI* strains, exponentially growing cells were grown in normal
441 YPD, then transferred into YPD (pH3.9), grown to $\sim 10^7$ cell/mL, and then synchronized in G1 with
442 three doses of α -factor at 2 μ g/mL at 0-, 50-, and 100-min time point at 30°C. Cells were collected at
443 150 min for release. To release from G1 arrest, cells were collected by filtration and promptly
444 washed twice on the filter using one culture volume of H₂O and then resuspended into YPD medium
445 containing 0.2 mg/mL pronase E (Sigma).

446
447 **Protein sample preparation and immunoblot analysis**
448 TCA extraction of yeast proteins was as described previously ((Sheu et al., 2014)). For immunoblot
449 analysis, protein samples were fractionated by SDS-PAGE and transferred to a nitrocellulose
450 membrane. Immunoblot analyses for Orc6 (SB49), Rad53 (ab104232, Abcam), γ -H2A (ab15083,
451 Abcam) and Sml1 (AS10 847, Agrisera) were performed as described ((Sheu et al., 2016, 2014)).
452

453
454
455 **Isolation and preparation of DNA for whole-genome replication profile analysis**
456 Modified protocol based on previously described ((Sheu et al., 2016, 2014)). Briefly, yeast cells
457 were synchronized in G1 with α -factor and released into medium containing 0.2 mg/mL pronase E,
458 0.5 mM 5-ethynyl-2'-deoxyuridine (EdU) with or without addition of 200 mM HU as indicated in the
459 main text. At the indicated time point, cells were collected for preparation of genomic DNA. The
460 genomic DNA were fragmented, biotinylated, and then purified. Libraries for Illumina sequencing
461 were constructed using TruSeq ChIP Library Preparation Kit (Illumina). Libraries were pooled and
462 submitted for 50 bp paired-end sequencing.
463

464 **Sample preparation for Chromatin immunoprecipitation coupled to deep sequencing (ChIP-
465 seq)**
466 Chromatin immunoprecipitation (ChIP) was performed as described ((Behrouzi et al., 2016)) with
467 modification. About 10^9 synchronized yeast cells were fixed with 1% formaldehyde for 15 min at
468 room temperature (RT), then quenched with 130 mM glycine for 5 min at RT, harvested by
469 centrifugation, washed twice with TBS (50 mM Tris.HCl pH 7.6, 150 mM NaCl), and flash frozen.
470 Cell pellets were resuspended in 600 μ l lysis buffer (50 mM HEPES-KOH pH 7.5, 150 mM NaCl, 1
471 mM EDTA, 1% Triton X-100, 0.1% Na-Deoxycholate, 0.1% SDS, 1 mM PMSF, protease inhibitor
472 tablet (Roche)), and disrupted by bead beating using multi-tube vortex (Multi-Tube Vortexer, Baxter
473 Scientific Products) for 12-15 cycles of 30 seconds vortex at maximum intensity. Cell extracts were
474 collected and sonicated using Bioruptor (UCD-200, Diagenode) for 38 cycles of pulse for 30
475 seconds "ON", 30 seconds "OFF" at amplitude setting High (H). The extract was centrifuged for 5
476 min at 14,000 rpm. The soluble chromatin was used for IP.
477

478 Antibodies against Cdc45 (CS1485, this lab (Sheu and Stillman, 2006)), Rad53 (ab104232, Abcam),
479 γ -H2A (ab15083, Abcam) was preincubated with washed Dynabeads Protein A/G (Invitrogen, 1002D
480 and 1004D). For each immunoprecipitation, 80 μ l antibody-coupled beads was added to soluble
481 chromatin. Samples were incubated overnight at 4°C with rotation, after which the beads were
482 collected on magnetic stands, and washed 3 times with 1 ml lysis buffer and once with 1 ml TE, and
483 eluted with 250 μ l preheated buffer (50 mM Tris.HCl pH 8.0, 10 mM EDTA, 1% SDS) at 65°C for
484 15 min. Immunoprecipitated samples were incubated overnight at 65°C to reverse crosslink, and

485 treated with 50 μ g RNase A at 37°C for 1 hr. 5 μ l proteinase K (Roche) was added and incubation
486 was continued at 55°C for 1 hr. Samples were purified using MinElute PCR purification kit
487 (Qiagen). Libraries for Illumina sequencing were constructed using TruSeq ChIP Library Preparation
488 Kit (Illumina, IP-202-1012 and IP-202-1024).

489
490 The duplicate Rad53 ChIP-Seq data was compared to published ChIP-Seq data for Swi6 (Park et al.,
491 2013) ([SRX360900](#): GSM1241092: swi6_DMSO_illumina; *Saccharomyces cerevisiae*; ChIP-Seq),
492 creating Gini indexes from calculated Lorenz curves (Andri et mult. al. S (2021). *DescTools: Tools*
493 *for Descriptive Statistics*. R package version 0.99.41, <https://cran.r-project.org/package=DescTools>).

494
495 **Sample preparation for RNA seq**
496 About 2-3x10⁸ flash-frozen yeast cells were resuspended in Trizol (cell pellet: Trizol = 1:10) and
497 vortex for 15 sec and incubate 25°C for 5 min. Add 200 μ l chloroform per 1 ml of Trizol-cell
498 suspension, vortex 15 sec, then incubate at room temp for 5 min and centrifuge to recover the
499 aqueous layer. The RNA in the aqueous layer were further purified and concentrated using PureLink
500 Column (Invitrogen, 12183018A). The RNA was eluted in 50 μ l and store at 20°C if not used
501 immediately. Store at -80°C for long term. Paired-end RNA-seq libraries were prepared using
502 TruSeq stranded mRNA library preparation kit (Illumina, 20020594).

503
504 **Generation of coverage tracks using the Galaxy platform**
505 For visualization of read coverage in the Integrated Genome Browser ((Freese et al., 2016)), the
506 coverage tracks were generated using the Galaxy platform maintained by the Bioinformatics Shared
507 Resource (BSR) of Cold Spring Harbor Lab. The paired-end reads from each library were trimmed to
508 31 bases and mapped to *sacCer3* genome using Bowtie ((Langmead, 2010)). The coverage track of
509 mapped reads was then generated using bamCoverage ((Ramírez et al., 2014)) with normalization to
510 1x genome.

511
512 **Definition of the origin-types**
513 Based on the BamCoverage output for EdU signal in *WT*, *rad53^{K227A}* and *mrc1 Δ* , we categorized 829
514 origins listed in the oriDB database ((Siow et al., 2012)). We define the early origins as the one whose
515 signal at the first time point is larger than 2. The late origins are extracted from the rest of the origins if the
516 average signal value at the later time point is larger than 2 in *rad53^{K227A}* and *mrc1 Δ* mutants. Among the
517 829 entries in oriDB, we defined 521 as active origins (with EdU signal in *WT* or checkpoint mutants
518 *rad53^{K227A}* and *mrc1 Δ*), in which 256 was categorized as early origins (with EdU signal in *WT*) and
519 265 as late origins (with signal in checkpoint mutants but not in *WT*). The remaining 308 entries do
520 not have significant signal under our condition and were deemed inactive origins.

521
522 **Computational analysis of sequence data**
523 The sequenced reads were trimmed by cutadapt with an option of “nextseq-trim”, then aligned by
524 STAR ((Dobin et al., 2013)) in a paired-end mode to the *sacCer3* genome masked at repetitive
525 regions. The gene structure is referred from SGD reference genome annotation R64.1.1 as of Oct.
526 2018. For RNA-seq quantification analysis, the total counts of aligned reads were computed for each
527 gene by applying “GeneCounts” mode. For ChIP-seq quantification analysis, the reads were mapped
528 using the same pipeline. Additionally, peak calling was done by MACS2 in a narrow peak mode.

529
530 **Gene expression analysis**

531 Differentially expressed genes (DEGs) and their p-values were computed for each pair of the cases by
532 `nbinomWaldTest` after size factor normalization using `DESeq2` ((Love et al., 2014)). Using the list of
533 DEGs, GO and KEGG enrichment analyses were performed via `Pathview` library. `ClusterProfiler`
534 was applied to visualize fold changes of DEGs in each KEGG pathway. Co-expression analysis of
535 significant DEGs was further performed base on co-expression network constructed in `CoCoCoNet`
536 ((Lee et al., 2020)). `CoCoCoNet` has established the co-expression matrix of Spearman's correlation
537 ranking based on 2,690 samples downloaded from SRA database. We carried out clustering for the
538 correlation matrix downloaded from `CoCoCoNet` (`yeast_metaAggnet`) by `dynamicTreeCut` in R (or
539 hierarchical clustering) to obtain at most 10 clusters. The enrichment analysis for the gene set of each
540 cluster was performed in the same way with RNA-seq analysis.

541

542 **ChIP-seq signal normalization**

543 For ChIP-seq signal normalization, two different methods were applied to different types of analysis.
544 For ChIP-seq residual analysis, we used simple normalization. In this process, each case sample is
545 compared with the corresponding control sample of DNA input to compute \log_2 fold changes within
546 each 25 bp window reciprocally scaled by multiplying the total read counts of another sample. Then,
547 the average of fold changes is computed for each duplicate. For ChIP-seq heatmap analysis, we
548 employed the origin-aware normalization to account for the higher background around origin region
549 as a result of DNA replication. In the origin-aware normalization, the same computation used in
550 simple normalization, or \log_2 fold change with scaling by the total read count, is independently
551 applied for the region proximal to the origins and others. For the heatmap presented in this paper, the
552 origin-proximal region is defined as the region within 5,000 bp upstream and downstream.

553

554 **Heatmap analyses at origins and TSS**

555 After the average fold change computation and normalization from ChIP-seq signals, the signal
556 strength is visualized around the target regions such as TSSs and replication origins are extracted
557 using `normalizeToMatrix` function in `EnrichedHeatmap` (window size is 25 bp and average mode is
558 `w0`). We ordered heatmaps to examine a different signal enrichment pattern for the characteristics of
559 each origin or gene. For the heatmap row of each origin is ordered by the assigned replication timing
560 for ChIP-seq signals around replication origins. The replication time for the origins are annotated
561 with the replication timing data published previously ((Yabuki et al., 2002)). From the estimated
562 replication time for each 1,000 bp window, we extracted the closest window from the center of each
563 replication origin and assigned it as the representative replication timing if their distance is no more
564 than 5,000 bp. Early and late origins groups are categorized according to the definition of the origin-
565 types using the replication profile data from this study. The final set of the replication origins used in
566 the heatmap analysis are obtained after filtering out the replication origins overlapped with any of 238
567 hyper-ChIPable regions defined in the previous study ((Teytelman et al., 2013)). In total, 167 early
568 and 231 late origins pass this filter and are used in the heatmaps analysis in this study. For heatmaps
569 of the ChIP-seq signals around TSS, we ordered genes based on RNA-seq fold changes for all DEGs
570 or per co-expression cluster of DEGs based on gene co-expression network constructed in
571 `CoCoCoNet` ((Lee et al., 2020)).

572

573 **ChIP-seq residual analysis**

574 To detect the time-dependent increase or decrease of Rad53 binding signals, we first focused on the
575 500 bp window upstream from each TSS and computed the sum of the fold change signals estimated
576 for each 25-bp window scaled by the window size as an activity of Rad53 binding for each gene. The

577 overall activity scores are varied for each time point probably because of the different Rad53 protein
578 level or other batch-specific reasons. To adjust such sample specific differences for a fair
579 comparison, a linear regression is applied for the activity scores of all genes between G1 and other
580 time points HU45 and HU90 using `lm` function in R. Then we selected top genes showing the
581 deviated signals from the overall tendency according to the absolute residual values between the
582 actual and predicted values, excluding the genes with signal value lower than -0.075 after scaling the
583 maximal signal to 1. Top 1,000 genes with the highest absolute residual values were selected from 2
584 sets of experiments. The common 435 genes among the duplicates were selected for further analysis.
585

586 **Data Availability**

587 All data supporting this work are available at public data sites. XXXX Source data are provide with
588 this paper. XXXXURL.

589

590 **Code Availability**

591 R scripts for the co-expression analyses including clustering and enrichment analysis are available at
592 https://github.com/carushi/yeast_coexp_analysis.

593

594

595 **Figure legends**

596

597 **Figure 1. DNA synthesis under stress caused by depletion of dNTP pool and during recovery** 598 **from the stress.**

599 **a**, Yeast cells were synchronized in G1-phase and released into YPD containing 0.2 M HU for 90
600 min. (Top panel) Replication profiles of Chromosome IV for the wild type (WT), *rad53^{K227A}* and
601 *mrc1Δ* mutants. (Bottom panel) Replication profiles of wild type (WT), *rad9Δ* and *rad53^{K227A}*
602 mutants. Red arrows point out some late origins. Ori-DB track indicate positions of replication
603 origins annotated in OriDB (Siow et al., 2012). **b**, Scatter plot of EdU signals from early (E), late (L)
604 and inactive (I) origins in *WT rad53^{K227A}* and *mrc1Δ* mutants. **c**, Scheme for accessing DNA synthesis
605 during recovery from HU stress. **d**, Cells that had progressed from G1 into S-phase in HU for 45 min.
606 were released from the HU block and DNA synthesis labeled with EdU during an additional 25 min
607 (HU→S25) or were continued in HU for another 45 min. and labeled with EdU (HU→HU45).
608 Replication profiles of Chromosome III is shown as an example.

609

610 **Figure 1 – figure supplement 1. DNA synthesis under stress caused by depletion of dNTP pool**
611 Yeast cells were synchronized in G1 phase and released into YPD containing 0.2 M HU for 45 and 90
612 min (HU45 and HU90, respectively). **a**, Replication profiles of Chromosome IV for the wild type
613 (WT) and *mrc1Δ* mutants and for the WT and *rad53^{K227A}* mutants. **b**, Replication profiles of
614 Chromosome III of *WT*, *rad9Δ* and *rad53^{K227A}* mutants at HU90. Red arrows point out some late
615 origins. Location of some heterochromatin regions are also indicated (black text and arrows).
616

617

617 **Figure 2. Replisome status and checkpoint signaling at replication origins under replication** 618 **stress**

619 Cells were synchronized in G1-phase and released into YPD containing 0.2 M HU for 45 and 90 min
620 (HU45 and HU90, respectively). *WT*, *rad53^{K227A}* and *mrc1Δ* mutant cells at stages of G1, HU45 and
621 HU90 were collected and processed for ChIP-seq analysis for distribution of Cdc45, γ -H2A and
622 Rad53 at genome locations. **a, c and e**, Coverage tracks of ChIP-seq signals generated from mapped

623 reads using BamCoverage with normalization of 1X genome size. **b, d and f**, Heatmaps of ChIP-seq
624 signal across 30 kb interval centered on active origins. Early origins (top panels) and late origins
625 (bottom panels) are ordered according to the associated replication timing data reported in a previous
626 study ((Yabuki et al., 2002)). **a**, Distribution of Cdc45 ChIP-seq signal on chromosome III. **b**,
627 Heatmaps of Cdc45 ChIP-seq signal around active origins. **c**, γ -H2A ChIP-seq signal on chromosome
628 III. **d**, Heatmaps of γ -H2A ChIP-seq signal around active origins. **e**, Rad53 ChIP-seq signal on
629 chromosome III. **f**, Heatmaps of Rad53 ChIP-seq signal around active origins.

630

631 **Figure 2 – figure supplement 1. Heatmaps of ChIP-seq signal across 30 kb centered on all**
632 **active origins**

633 Cells were synchronized in G1 phase and released into YPD containing 0.2 M HU for 45 and 90 min
634 (HU45 and HU90, respectively). *WT*, *rad53^{K227A}* and *mrc1 Δ* mutant cells at stages of G1, HU45 and
635 HU90 were collected and processed for ChIP-seq analysis. **a, b, and c**, Heatmaps of ChIP-seq signal
636 of Cdc45, γ -H2A and Rad53, respectively, across 30 kb centered on all active origins as defined in
637 this study (see **Definition of the origin-types in methods section**). Origins are ordered according to
638 the associated replication timing data reported in previous study (Yabuki et al., 2002).

639

640 **Figure 3. Rad53 is recruited to TSS and the binding changes with the cell cycle stage**

641 **a**, Distribution of Rad53 ChIP-seq signal near *RNR1*, *PCL1* and *TOS6* genes in *WT*, *rad53^{K227A}* and
642 *mrc1 Δ* mutant cells at stages of G1, HU45 and HU90. **b**, Rad53 ChIP-seq profiles in *WT*, *sml1 Δ* ,
643 *rad53 Δ sml1 Δ* , and *mec1 Δ sml1 Δ* near *RNR1* gene. Asynchronous yeast cultures were processed for
644 ChIP-seq analysis for distribution of Rad53. Tracks from *WT* G1, HU45 and HU90 are also included
645 for reference. **c**, Heatmaps and average signals of Rad53 ChIP-seq signal across 2 kb interval
646 centered on transcription start sites (TSS) for *WT*, *rad53^{K227A}* and *mrc1 Δ* mutant cells at stages of G1,
647 HU45 and HU90.

648

649 **Figure 3 – figure supplement 1. Recruitment of Rad53 to upstream TSS depends on the**
650 **presence of Rad53**

651 **a**. Rad53 ChIP-seq profiles in *WT*, *sml1 Δ* , *rad53 Δ sml1 Δ* , and *mec1 Δ sml1 Δ* for chromosome III.
652 Asynchronous yeast cultures were processed for ChIP-seq analysis for distribution of Rad53. The
653 results from two independent experiments are shown. Experiment 1 compares only *sml1 Δ* ,
654 *rad53 Δ sml1 Δ* . Experiment 2 is the same shown in Figure 3b. Tracks from *WT* G1, HU45 and HU90
655 are also included for reference. **b**, Pie charts showing the distribution of Rad53 ChIP-seq peaks in
656 relation to genes.

657

658 **Figure 3 – figure supplement 2. Relative level of Rad53 protein changes in cells**

659 **a**, Immunoblots monitoring protein status for Rad53, Orc6, γ -H2A and Sml1 during checkpoint
660 activation from G1 to HU45 and HU90. **b**, Comparison of Rad53 protein level in G1 extracts from
661 *WT*, *rad53^{K227A}*, *mrc1 Δ* and *rad9 Δ* cells. Blots for Orc6, γ -H2A and Sml1 are included for reference.
662 **c**, Comparison of Rad53 protein level in HU90 extracts from *WT*, *rad53^{K227A}*, *mrc1 Δ* and *rad9 Δ* cells.
663 14 % SDS-PAGE was used for the Rad53 blot to allow collapsing of all phosphorylated forms into a
664 single band. Two-fold dilutions of the samples are loaded.

665

666 **Figure 4. Identification of genes with Rad53 binding changes at the promoters**

667 **a**. Examples of coverage tracks for selected genes show Rad53 signal changes at the indicated
668 promoters from G1 to HU. **(b)** Scatter plots compare the signals in G1 and HU45 at 500 bp intervals

669 upstream of TSS for all genes in WT. Orange dots indicated the 1000 genes with highest binding
670 changes (Top 1000 DB) and satisfying the filter of minimal signal of -0.075 (Maximal = 1). The two
671 plots represent WT data sets from two separate experiments (see text). (c) Binding changes for 435
672 genes that are in both sets of Top 1000 DB (435 Top DB overlap).

673
674 **Figure 5. Gene expression changes in WT and checkpoint mutants under stress and the**
675 **tendency of higher Rad53 binding at promoter of genes with significant differential expression**
676 **a.** Rank data analysis of RNA-seq samples. *WT*, *rad9Δ*, *rad53^{K227A}* and *mrc1Δ* cells were
677 synchronized in G1-phase and released into YPD containing 0.2 M HU for 45 and 90 min (HU45 and
678 HU90, respectively). Cells at stages of G1, HU45 and HU90 were collected and processed for RNA-
679 seq analysis. (b) Bar graph summarizing the number of genes that show statistically significant
680 differential expression (DEGs) in pair-wise comparison as indicated to the right. Blue bars, down-
681 regulated DEGs. Orange bars, up-regulated DEGs. (c) Average Rad53 ChIP-seq signal across 2 kb
682 interval centered on at TSS for statistically significant (red) and insignificant (cyan) DEGs.

683
684 **Figure 5 – figure supplement 1. Average Rad53 ChIP-seq signal and heatmaps of signal across**
685 **2 kb interval centered on TSS for various groups of time-dependent differentially expressed**
686 **genes (DEGs)**

687 **a,** Rad53 ChIP-seq signal in *WT*, *rad53^{K227A}* and *mrc1Δ* mutant cells at stages G1, HU45 and HU90
688 for DEGs in WT(G1→HU45) and in WT(G1→HU90). **b and c,** Rad53 ChIP-seq signal DEGs in
689 *rad53^{K227A}*(G1→HU45) and *mrc1Δ*(G1→HU45), respectively. Genes in each group are arranged
690 according to the differential expression level from up to down. Average ChIP-seq signal for
691 significant (red) and for insignificant (cyan) DEGs are plotted on top of the heatmap.

692
693 **Figure 6. Correlation between differential binding of Rad53 at promoter and differential gene**
694 **expression**

695 **a,** Co-expression cluster matrix for significant DEGs in WT (G1→HU45). Cluster (C): color codes
696 for DEG clusters. Gene(G): level of differential expression. **b,** Heatmaps of Rad53 ChIP-seq signal
697 across 2 kb interval centered on TSS for DEG clusters in **a.** Genes within each cluster are ordered by
698 the level of expression changes from up to down. **c,** Scatter plots of binding changes against
699 expression changes for the 236 significant DEGs in the 435 Top DB overlap group (top, left) and
700 subgroups in clusters 1, 2, 4 and 7.

701
702 **Figure 6 – figure supplement 1. Rad53 ChIP-seq signal and heatmaps of signal across 2 kb**
703 **interval centered on TSS for co-expression clusters in significant DEG in WT (G1→HU45).**
704 Genes in each group are arranged according to the log₂ based differential expression level from up to
705 down. The three left most heatmap columns for WT samples are identical as in Figure 6b.

706
707 **Figure 7. Origin-proximal DEGs are biased towards down-regulation in the *mrc1Δ* mutant.**
708 **a,** Co-expression cluster matrix for significant DEGs in HU45 (*mrc1Δ* vs *WT*). Cluster (C): color
709 codes for DEG clusters. Gene(G): level of differential expression. **b,** Heatmaps of Rad53 ChIP-seq
710 signal across 2 kb interval centered on TSS for DEG clusters in **a.** ChIP-seq signal in *WT*, *rad53^{K227A}*
711 and *mrc1Δ* mutant cells at stages G1, HU45 and HU90 are shown. **c,** Summary of gene-origin
712 relation in DEGs co-expression clusters for HU45 (*mrc1Δ* vs *WT*). Distance between each TSS and
713 its nearest origin center is indicated in pink gradient as well as light purple (<2 kb) and dark purple
714 (<1 kb). Relative TSS-origin orientation and origin type are indicated. **d,** Proportion of down/up

715 regulation of DEGs as categorized by TSS to origin distance (left panels), origin type within 5 kb
716 (middle panels) and orientation (right panels; CD: co-directional; HO: head-on).

717
718 **Figure 7 – figure supplement 1. Origin-proximal DEGs are biased towards down-regulation in**
719 **the *rad53^{K227A}* mutant.**

720 **a.** Co-expression cluster matrix for significant DEGs in HU45 (*rad53^{K227A}* vs *WT*). Cluster (C): color
721 codes for DEG clusters. Gene(G): level of differential expression. **b,** Heatmaps of Rad53 ChIP-seq
722 signal across 2 kb interval centered on TSS for DEG clusters above. ChIP-seq signal in *WT*,
723 *rad53^{K227A}* and *mrc1Δ* mutant cells at stages G1, HU45 and HU90 are shown. **c,** Summary of gene-
724 origin relation in DEGs co-expression clusters for HU45(*rad53^{K227A}* vs *WT*). Distance between each
725 TSS and its nearest origin center is indicated in pink gradient as well as light purple (<2 kb) and dark
726 purple (<1 kb). Relative TSS-origin orientation and origin type are indicated.

727
728 **Figure 8. SBF plays a major role in the localization of Rad53 to the promoters of its target**
729 **genes under replication stress**

730 Differential binding of Rad53 at promoters and differential expression of target genes of SBF, MBF,
731 Msn4 and Ste12. **a,** Top panels: scatter plots of binding changes (DB residual) and expression
732 changes (log₂ Fold change) for targets of indicated transcription regulators that are in the 236
733 significant DEGs in the Top DB overlap (Figure 4). Bottom panels: scatter plots above adding the
734 expression change data from the checkpoint mutants. Enrichment of transcription regulator targets in
735 the 236 Top DB DEGs. **b,** Top panels: Scatter plots illustrating the Rad53 signal upstream of TSS for
736 all genes in *WT*, *ixr1Δ*, *swi4Δ* and *swi6Δ* mutants. SBF targets found in the 435 Top DB overlap are
737 show as orange or red diamond and *RNR1* in red diamond. Bottom panels: Close-up for specific area
738 from above panels. **c,** Distribution of Rad53 ChIP-seq signal near selected Top DB genes that are
739 targets of SBF, MBF, Ixr1 or Rfx1 in *WT*, *ixr1Δ*, *swi4Δ* and *swi6Δ* mutants at stages of G1, HU45
740 and HU90.

741
742 **Figure 8 – figure supplement 1. Differential binding of Rad53 at promoter and differential**
743 **expression of target genes of SBF, MBF, Msn4 and Ste12.**

744 **a, b, c and d,** Targets of SBF, MBF, Ste12 and Msn4, respectively. Scatter plots of binding changes
745 (DB residual) and expression changes (log₂ Fold change) for targets of indicated transcription
746 regulators that are in the 236 significant DEGs in the Top DB overlap. Expression change data from
747 *WT*, *rad53^{K227A}*, *mrc1Δ* and *rad9Δ* are presented in pairwise manner for comparison and column
748 graphs of expression change data from *WT*, *rad53^{K227A}*, *mrc1Δ* and *rad9Δ* cells for genes presented in
749 the scatter plots above.

750

751 **References**

752
753

754 Alepuz PM, Jovanovic A, Reiser V, Ammerer G. 2001. Stress-Induced MAP Kinase Hog1 Is Part of
755 Transcription Activation Complexes. *Mol Cell* **7**:767–777. doi:10.1016/s1097-2765(01)00221-0

756 Bacal J, Carretero MM, Pardo B, Barthe A, Sharma S, Chabes A, Lengronne A, Pasero P. 2018. Mrc1
757 and Rad9 cooperate to regulate initiation and elongation of DNA replication in response to DNA
758 damage. *The EMBO journal* e99319. doi:10.15252/embj.201899319

759 Bastos de Oliveira FM, Kim D, Cussiol JR, Das J, Jeong MC, Doerfler L, Schmidt KH, Yu H,
760 Smolka MB. 2015. Phosphoproteomics Reveals Distinct Modes of Mec1/ATR Signaling during
761 DNA Replication. *Mol Cell* **57**:1124–1132. doi:10.1016/j.molcel.2015.01.043

762 Behrouzi R, Lu C, Currie M, Jih G, Iglesias N, Moazed D. 2016. Heterochromatin assembly by
763 interrupted Sir3 bridges across neighboring nucleosomes. *Elife* **5**:e17556. doi:10.7554/elife.17556

764 Bell SP, Labib K. 2016. Chromosome Duplication in *Saccharomyces cerevisiae*. *Genetics* **203**:1027–
765 1067. doi:10.1534/genetics.115.186452

766 Bermejo R, Capra T, Jossen R, Colosio A, Frattini C, Carotenuto W, Cocito A, Doksani Y, Klein H,
767 Gómez-González B, Aguilera A, Katou Y, Shirahige K, Foiani M. 2011. The Replication
768 Checkpoint Protects Fork Stability by Releasing Transcribed Genes from Nuclear Pores. *Cell*
769 **146**:233–246. doi:10.1016/j.cell.2011.06.033

770 Breeden LL. 2003. Periodic Transcription: A Cycle within a Cycle. *Curr Biol* **13**:R31–R38.
771 doi:10.1016/s0960-9822(02)01386-6

772 Bruhn C, Ajazi A, Ferrari E, Lanz MC, Batrin R, Choudhary R, Walvekar A, Laxman S, Longhese
773 MP, Fabre E, Smolka MB, Foiani M. 2020. The Rad53CHK1/CHK2-Spt21NPAT and Tel1ATM
774 axes couple glucose tolerance to histone dosage and subtelomeric silencing. *Nat Commun*
775 **11**:4154. doi:10.1038/s41467-020-17961-4

776 Bruin RAM de, Kalashnikova TI, Chahwan C, McDonald WH, Wohlschlegel J, Yates J, Russell P,
777 Wittenberg C. 2006. Constraining G1-Specific Transcription to Late G1 Phase: The MBF-
778 Associated Corepressor Nrm1 Acts via Negative Feedback. *Mol Cell* **23**:483–496.
779 doi:10.1016/j.molcel.2006.06.025

780 Callegari AJ, Kelly TJ. 2006. UV irradiation induces a postreplication DNA damage checkpoint.
781 *Proc National Acad Sci* **103**:15877–15882. doi:10.1073/pnas.0607343103

782 Can G, Kauerhof AC, Macak D, Zegerman P. 2018. Helicase Subunit Cdc45 Targets the Checkpoint
783 Kinase Rad53 to Both Replication Initiation and Elongation Complexes after Fork Stalling. *Mol*
784 *Cell* **73**. doi:10.1016/j.molcel.2018.11.025

- 785 Cobb JA, Schleker T, Rojas V, Bjergbaek L, Tercero JA, Gasser SM. 2005. Replisome instability,
786 fork collapse, and gross chromosomal rearrangements arise synergistically from Mec1 kinase and
787 RecQ helicase mutations. *Genes & Development* **19**:3055–3069. doi:10.1101/gad.361805
- 788 Desany BA, Alcasabas AA, Bachant JB, Elledge SJ. 1998. Recovery from DNA replicational stress is
789 the essential function of the S-phase checkpoint pathway. *Gene Dev* **12**:1–15.
790 doi:10.1101/gad.12.18.2956
- 791 Devbhandari S, Remus D. 2020. Rad53 limits CMG helicase uncoupling from DNA synthesis at
792 replication forks. *Nat Struct Mol Biol* **27**:461–471. doi:10.1038/s41594-020-0407-7
- 793 Dobin A, Davis CA, Schlesinger F, Drenkow J, Zaleski C, Jha S, Batut P, Chaisson M, Gingeras TR.
794 2013. STAR: ultrafast universal RNA-seq aligner. *Bioinformatics* **29**:15–21.
795 doi:10.1093/bioinformatics/bts635
- 796 Forey R, Poveda A, Sharma S, Barthe A, Padioleau I, Renard C, Lambert R, Skrzypczak M, Ginalski
797 K, Lengronne A, Chabes A, Pardo B, Pasero P. 2020. Mec1 Is Activated at the Onset of Normal S
798 Phase by Low-dNTP Pools Impeding DNA Replication. *Molecular Cell*.
799 doi:10.1016/j.molcel.2020.02.021
- 800 Freese NH, Norris DC, Loraine AE. 2016. Integrated genome browser: visual analytics platform for
801 genomics. *Bioinformatics* **32**:2089–2095. doi:10.1093/bioinformatics/btw069
- 802 Gilbert CS, Green CM, Lowndes NF. 2001. Budding Yeast Rad9 Is an ATP-Dependent Rad53
803 Activating Machine. *Mol Cell* **8**:129–136. doi:10.1016/s1097-2765(01)00267-2
- 804 Gradolatto A, Rogers RS, Lavender H, Taverna SD, Allis CD, Aitchison JD, Tackett AJ. 2008.
805 *Saccharomyces cerevisiae* Yta7 Regulates Histone Gene Expression. *Genetics* **179**:291–304.
806 doi:10.1534/genetics.107.086520
- 807 Gunjan A, Verreault A. 2003. A Rad53 kinase-dependent surveillance mechanism that regulates
808 histone protein levels in *S. cerevisiae*. *Cell* **115**:537–549. doi:10.1016/s0092-8674(03)00896-1
- 809 Hamperl S, Cimprich KA. 2016. Conflict Resolution in the Genome: How Transcription and
810 Replication Make It Work. *Cell* **167**:1455–1467. doi:10.1016/j.cell.2016.09.053
- 811 Hoch NC, Chen ESW, Buckland R, Wang S-C, Fazio A, Hammet A, Pelliccioli A, Chabes A, Tsai M-
812 D, Heierhorst J. 2013. Molecular basis of the essential s phase function of the rad53 checkpoint
813 kinase. *Molecular and Cellular Biology* **33**:3202–3213. doi:10.1128/mcb.00474-13
- 814 Holzen TM, Sclafani RA. 2010. Genetic interaction of RAD53 protein kinase with histones is
815 important for DNA replication. *Cell Cycle* **9**:4735–4747. doi:10.4161/cc.9.23.14091
- 816 Huang M, Zhou Z, Elledge SJ. 1998. The DNA Replication and Damage Checkpoint Pathways
817 Induce Transcription by Inhibition of the Crt1 Repressor. *Cell* **94**:595–605. doi:10.1016/s0092-
818 8674(00)81601-3

- 819 Jaehnig EJ, Kuo D, Hombauer H, Ideker TG, Kolodner RD. 2013. Checkpoint kinases regulate a
820 global network of transcription factors in response to DNA damage. *Cell reports* **4**:174–188.
821 doi:10.1016/j.celrep.2013.05.041
- 822 Kim K-Y, Truman AW, Levin DE. 2008. Yeast Mpk1 Mitogen-Activated Protein Kinase Activates
823 Transcription through Swi4/Swi6 by a Noncatalytic Mechanism That Requires Upstream Signal
824 †. *Mol Cell Biol* **28**:2579–2589. doi:10.1128/mcb.01795-07
- 825 Kumar S, Huberman JA. 2008. Checkpoint-Dependent Regulation of Origin Firing and Replication
826 Fork Movement in Response to DNA Damage in Fission Yeast †. *Mol Cell Biol* **29**:602–611.
827 doi:10.1128/mcb.01319-08
- 828 Langmead B. 2010. Aligning Short Sequencing Reads with Bowtie. *Curr Protoc Bioinform*
829 **32**:11.7.1-11.7.14. doi:10.1002/0471250953.bi1107s32
- 830 Lanz MC, Dibitetto D, Smolka MB. 2019. DNA damage kinase signaling: checkpoint and repair at 30
831 years. *Embo J* **38**:e101801. doi:10.15252/embj.2019101801
- 832 Lao JP, Ulrich KM, Johnson JR, Newton BW, Vashisht AA, Wohlschlegel JA, Krogan NJ, Toczyski
833 DP. 2018. The Yeast DNA Damage Checkpoint Kinase Rad53 Targets the Exoribonuclease, Xrn1.
834 *G3 Genes Genomes Genetics* **8**:g3.200767.2018. doi:10.1534/g3.118.200767
- 835 Lee J, Shah M, Ballouz S, Crow M, Gillis J. 2020. CoCoCoNet: conserved and comparative co-
836 expression across a diverse set of species. *Nucleic Acids Res* **48**:gkaa348-
837 doi:10.1093/nar/gkaa348
- 838 Lopes M, Cotta-Ramusino C, Pelliccioli A, Liberi G, Plevani P, Muzi-Falconi M, Newlon CS, Foiani
839 M. 2001. The DNA replication checkpoint response stabilizes stalled replication forks. *Nature*
840 **412**:557–561. doi:10.1038/35087613
- 841 Lou H, Komata M, Katou Y, Guan Z, Reis CC, Budd M, Shirahige K, Campbell JL. 2008. Mrc1 and
842 DNA polymerase epsilon function together in linking DNA replication and the S phase
843 checkpoint. *Molecular Cell* **32**:106–117. doi:10.1016/j.molcel.2008.08.020
- 844 Love MI, Huber W, Anders S. 2014. Moderated estimation of fold change and dispersion for RNA-
845 seq data with DESeq2. *Genome Biol* **15**:550. doi:10.1186/s13059-014-0550-8
- 846 Manfrini N, Gobbin E, Baldo V, Trovesi C, Lucchini G, Longhese MP. 2012. G1/S and G2/M
847 Cyclin-Dependent Kinase Activities Commit Cells to Death in the Absence of the S-Phase
848 Checkpoint. *Mol Cell Biol* **32**:4971–4985. doi:10.1128/mcb.00956-12
- 849 McClure AW, Diffley J. 2021. Rad53 checkpoint kinase regulation of DNA replication fork rate via
850 Mrc1 phosphorylation. doi:10.1101/2021.04.09.439171

- 851 Oliveira FMB de, Harris MR, Brazauskas P, Bruin RAM de, Smolka MB. 2012. Linking DNA
852 replication checkpoint to MBF cell-cycle transcription reveals a distinct class of G1/S genes. *The*
853 *EMBO Journal* **31**:1798–1810. doi:10.1038/emboj.2012.27
- 854 Osborn AJ, Elledge SJ. 2003. Mrc1 is a replication fork component whose phosphorylation in
855 response to DNA replication stress activates Rad53. *Gene Dev* **17**:1755–1767.
856 doi:10.1101/gad.1098303
- 857 Pardo B, Crabbé L, Pasero P. 2017. Signaling pathways of replication stress in yeast. *FEMS Yeast*
858 *Research* **17**. doi:10.1093/femsyr/fow101
- 859 Park D, Lee Y, Bhupindersingh G, Iyer VR. 2013. Widespread Misinterpretable ChIP-seq Bias in
860 Yeast. *Plos One* **8**:e83506. doi:10.1371/journal.pone.0083506
- 861 Paulovich AG, Hartwell LH. 1995. A checkpoint regulates the rate of progression through S phase in
862 *S. cerevisiae* in Response to DNA damage. *Cell* **82**:841–847. doi:10.1016/0092-8674(95)90481-6
- 863 Pelliccioli A, Lucca C, Liberi G, Marini F, Lopes M, Plevani P, Romano A, Fiore PPD, Foiani M.
864 1999. Activation of Rad53 kinase in response to DNA damage and its effect in modulating
865 phosphorylation of the lagging strand DNA polymerase. *The EMBO Journal* **18**:6561–6572.
866 doi:10.1093/emboj/18.22.6561
- 867 Ramírez F, Dünder F, Diehl S, Grüning BA, Manke T. 2014. deepTools: a flexible platform for
868 exploring deep-sequencing data. *Nucleic Acids Res* **42**:W187–W191. doi:10.1093/nar/gku365
- 869 Renard-Guillet C, Kanoh Y, Shirahige K, Masai H. 2014. Temporal and spatial regulation of
870 eukaryotic DNA replication: From regulated initiation to genome-scale timing program. *Semin*
871 *Cell Dev Biol* **30**:110–120. doi:10.1016/j.semcdb.2014.04.014
- 872 Saldivar JC, Cortez D, Cimprich KA. 2017. The essential kinase ATR: ensuring faithful duplication
873 of a challenging genome. *Nature Publishing Group* **16**:1–15. doi:10.1038/nrm.2017.67
- 874 Sanz AB, García R, Rodríguez-Peña JM, Nombela C, Arroyo J. 2018. Slt2 MAPK association with
875 chromatin is required for transcriptional activation of Rlm1 dependent genes upon cell wall stress.
876 *Biochimica Et Biophysica Acta Bba - Gene Regul Mech* **1861**:1029–1039.
877 doi:10.1016/j.bbagr.2018.09.005
- 878 Seiler JA, Conti C, Syed A, Aladjem MI, Pommier Y. 2007. The Intra-S-Phase Checkpoint Affects
879 both DNA Replication Initiation and Elongation: Single-Cell and -DNA Fiber Analyses ▽. *Mol*
880 *Cell Biol* **27**:5806–5818. doi:10.1128/mcb.02278-06
- 881 Sheu Y-J, Kinney JB, Lengronne A, Pasero P, Stillman B. 2014. Domain within the helicase subunit
882 Mcm4 integrates multiple kinase signals to control DNA replication initiation and fork
883 progression. *Proceedings of the National Academy of Sciences* **111**:E1899-908.
884 doi:10.1073/pnas.1404063111

- 885 Sheu Y-J, Kinney JB, Stillman B. 2016. Concerted activities of Mcm4, Sld3, and Dbf4 in control of
886 origin activation and DNA replication fork progression. *Genome Research* **26**:315–330.
887 doi:10.1101/gr.195248.115
- 888 Sheu Y-J, Stillman B. 2006. Cdc7-Dbf4 phosphorylates MCM proteins via a docking site-mediated
889 mechanism to promote S phase progression. *Mol Cell* **24**:101–113.
890 doi:10.1016/j.molcel.2006.07.033
- 891 Sidorova JM, Breeden LL. 2003. Rad53 Checkpoint Kinase Phosphorylation Site Preference
892 Identified in the Swi6 Protein of *Saccharomyces cerevisiae*. *Mol Cell Biol* **23**:3405–3416.
893 doi:10.1128/mcb.23.10.3405-3416.2003
- 894 Siow CC, Nieduszynska SR, Müller CA, Nieduszynski CA. 2012. OriDB, the DNA replication origin
895 database updated and extended. *Nucleic Acids Res* **40**:D682–D686. doi:10.1093/nar/gkr1091
- 896 Smolka MB, Albuquerque CP, Chen S, Zhou H. 2007. Proteome-wide identification of in vivo targets
897 of DNA damage checkpoint kinases. *Proceedings of the National Academy of Sciences of the*
898 *United States of America* **104**:10364–10369. doi:10.1073/pnas.0701622104
- 899 Smolka MB, Chen S, Maddox PS, Enserink JM, Albuquerque CP, Wei XX, Desai A, Kolodner RD,
900 Zhou H. 2006. An FHA domain-mediated protein interaction network of Rad53 reveals its role in
901 polarized cell growth. *The Journal of Cell Biology* **175**:743–753. doi:10.1083/jcb.200605081
- 902 Szyjka SJ, Aparicio JG, Viggiani CJ, Knott S, Xu W, Tavaré S, Aparicio OM. 2008. Rad53 regulates
903 replication fork restart after DNA damage in *Saccharomyces cerevisiae*. *Gene Dev* **22**:1906–1920.
904 doi:10.1101/gad.1660408
- 905 Tercero JA, Longhese MP, Diffley JFX. 2003. A Central Role for DNA Replication Forks in
906 Checkpoint Activation and Response. *Mol Cell* **11**:1323–1336. doi:10.1016/s1097-
907 2765(03)00169-2
- 908 Teytelman L, Thurtle DM, Rine J, Oudenaarden A van. 2013. Highly expressed loci are vulnerable to
909 misleading ChIP localization of multiple unrelated proteins. *Proc National Acad Sci* **110**:18602–
910 18607. doi:10.1073/pnas.1316064110
- 911 Tourrière H, Versini G, Cerdón-Preciado V, Alabert C, Pasero P. 2005. Mrc1 and Tof1 promote
912 replication fork progression and recovery independently of Rad53. *Molecular Cell* **19**:699–706.
- 913 Travesa A, Kuo D, Bruin RAM de, Kalashnikova TI, Guaderrama M, Thai K, Aslanian A, Smolka
914 MB, Yates JR, Ideker T, Wittenberg C. 2012. DNA replication stress differentially regulates G1/S
915 genes via Rad53-dependent inactivation of Nrm1. *The EMBO Journal* **31**:1811–1822.
916 doi:10.1038/emboj.2012.28
- 917 Tsaponina O, Barsoum E, Aström SU, Chabes A. 2011. Ixr1 is required for the expression of the
918 ribonucleotide reductase Rnr1 and maintenance of dNTP pools. *PLoS Genetics* **7**:e1002061.
919 doi:10.1371/journal.pgen.1002061

- 920 Viggiani CJ, Aparicio OM. 2006. New vectors for simplified construction of BrdU-Incorporating
921 strains of *Saccharomyces cerevisiae*. *Yeast* **23**:1045–1051. doi:10.1002/yea.1406
- 922 Yabuki N, Terashima H, Kitada K. 2002. Mapping of early firing origins on a replication profile of
923 budding yeast. *Genes Cells* **7**:781–789. doi:10.1046/j.1365-2443.2002.00559.x
- 924 Yeeles JTP, Janska A, Early A, Diffley JFX. 2016. How the Eukaryotic Replisome Achieves Rapid
925 and Efficient DNA Replication. *Molecular Cell*. doi:10.1016/j.molcel.2016.11.017
- 926 Zhao X, Georgieva B, Chabes A, Domkin V, Ippel JH, Schleucher J, Wijmenga S, Thelander L,
927 Rothstein R. 2000. Mutational and Structural Analyses of the Ribonucleotide Reductase Inhibitor
928 Sml1 Define Its Rnr1 Interaction Domain Whose Inactivation Allows Suppression of *mec1* and
929 *rad53* Lethality. *Mol Cell Biol* **20**:9076–9083. doi:10.1128/mcb.20.23.9076-9083.2000
- 930
931

932 **Supplemental Table 1**
 933 Yeast strains used in this study

Strain	genotype	source
YS2571	<i>MATa bar1Δ::TRP1 URA3::BrdU-Inc ade2-1 can1-100 his3-11,-15 leu2-3,112 trp1-1 ura3-1</i>	Sheu et al 2014(Sheu et al., 2014)
YS3110	<i>MATa rad53^{K227A}::KanMX4 bar1Δ::TRP1 URA3::BrdU-Inc ade2-1 can1-100 his3-11,-15 leu2-3,112 trp1-1 ura3-1</i>	This study
YS3285	<i>MATa mrc1Δ::KanMX4 bar1Δ::TRP1 URA3::BrdU-Inc ade2-1 can1-100 his3-11,-15 leu2-3,112 trp1-1 ura3-1</i>	This study
YS3382	<i>MATa rad9Δ::HIS3 bar1Δ::TRP1 URA3::BrdU-Inc ade2-1 can1-100 his3-11,-15 leu2-3,112 trp1-1 ura3-1</i>	This study
YS3388	<i>MATa ixr1Δ::HIS3 bar1Δ::TRP1 URA3::BrdU-Inc ade2-1 can1-100 his3-11,-15 leu2-3,112 trp1-1 ura3-1</i>	This study
YS3401	<i>MATa swi4Δ::HIS3 bar1Δ::TRP1 URA3::BrdU-Inc ade2-1 can1-100 his3-11,-15 leu2-3,112 trp1-1 ura3-1</i>	This study
YS3406	<i>MATa swi6Δ::HIS3 bar1Δ::TRP1 URA3::BrdU-Inc ade2-1 can1-100 his3-11,-15 leu2-3,112 trp1-1 ura3-1</i>	This study
YS2828	<i>MATa URA3::BrdU-Inc ade2-1 can1-100 his3-11,-15 leu2-3,112 trp1-1 ura3-1</i>	Sheu et al 2016(Sheu et al., 2016)
YS3066	<i>MATa sml1Δ::HIS3 URA3::BrdU-Inc ade2-1 can1-100 his3-11,-15 leu2-3,112 trp1-1 ura3-1</i>	Sheu et al 2016(Sheu et al., 2016)
YS3075	<i>MATa mec1Δ::TRP1 sml1Δ::HIS3 URA3::BrdU-Inc ade2-1 can1-100 his3-11,-15 leu2-3,112 trp1-1 ura3-1</i>	Sheu et al 2016(Sheu et al., 2016)
YS3077	<i>MATa rad53Δ::KanMX sml1Δ::HIS3 URA3::BrdU-Inc ade2-1 can1-100 his3-11,-15 leu2-3,112 trp1-1 ura3-1</i>	Sheu et al 2016(Sheu et al., 2016)

934
 935

Figure 1

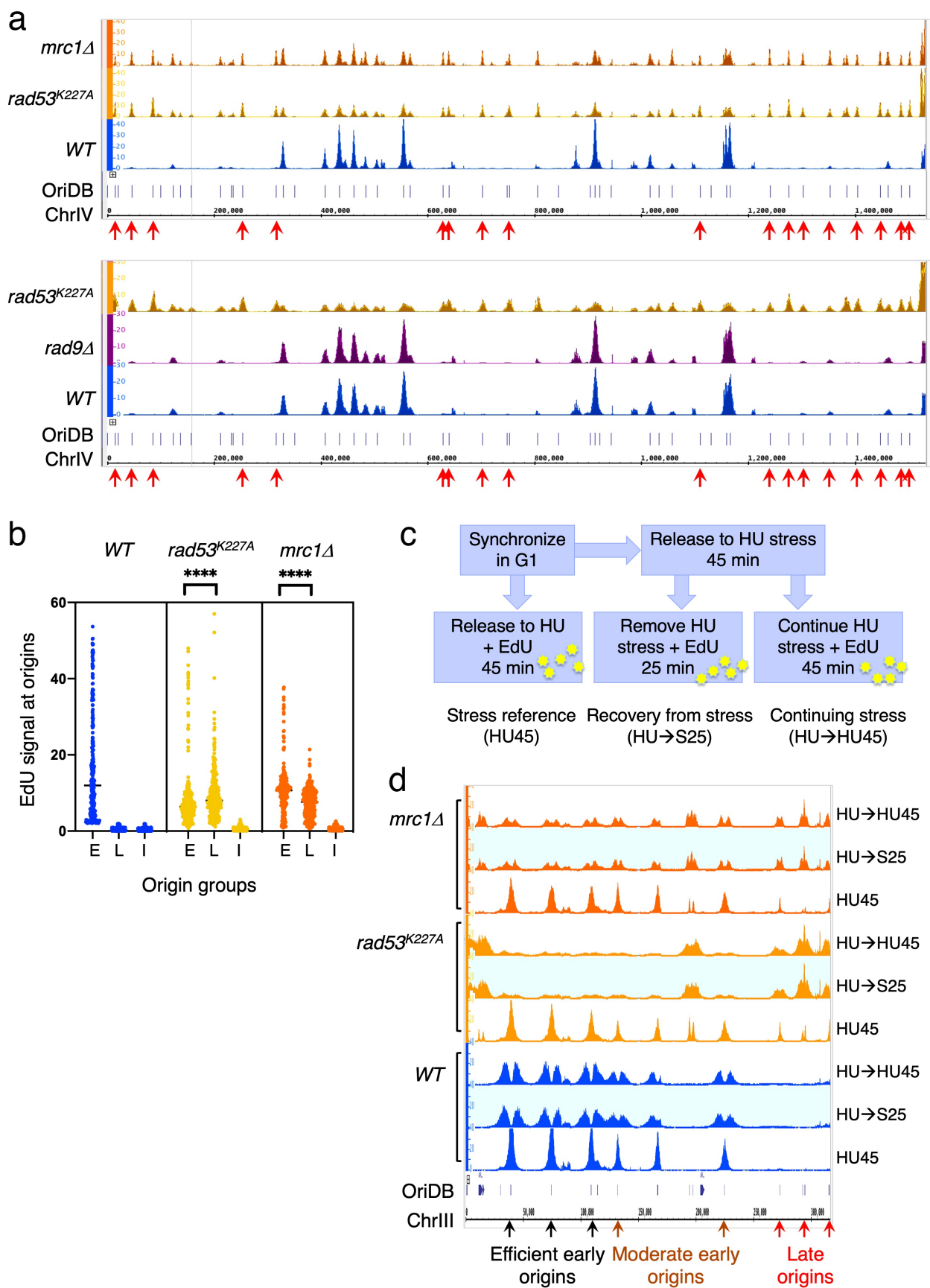
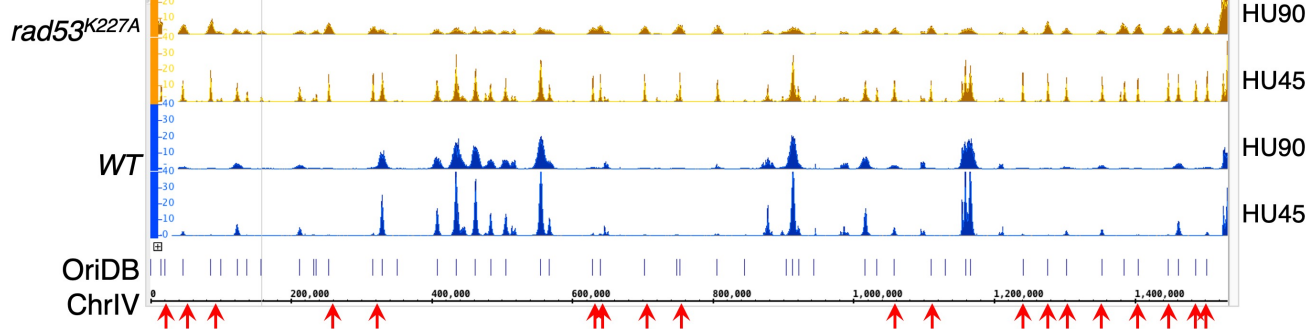
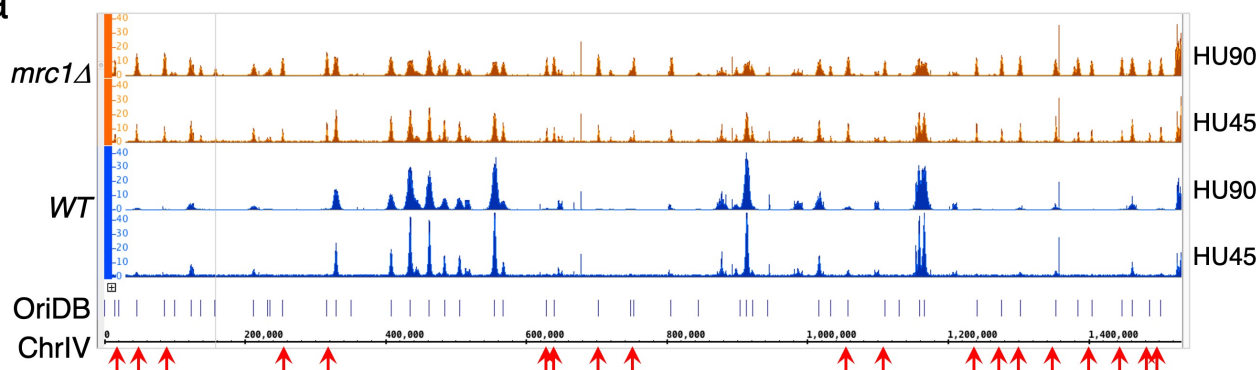


Figure 1 - figure supplement

a



b

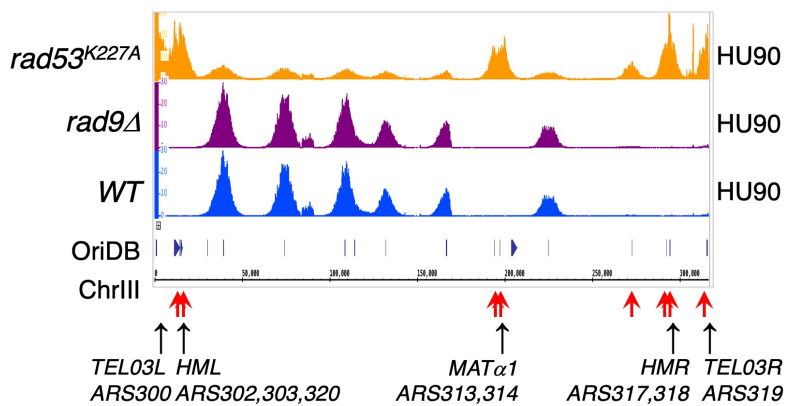


Figure 2

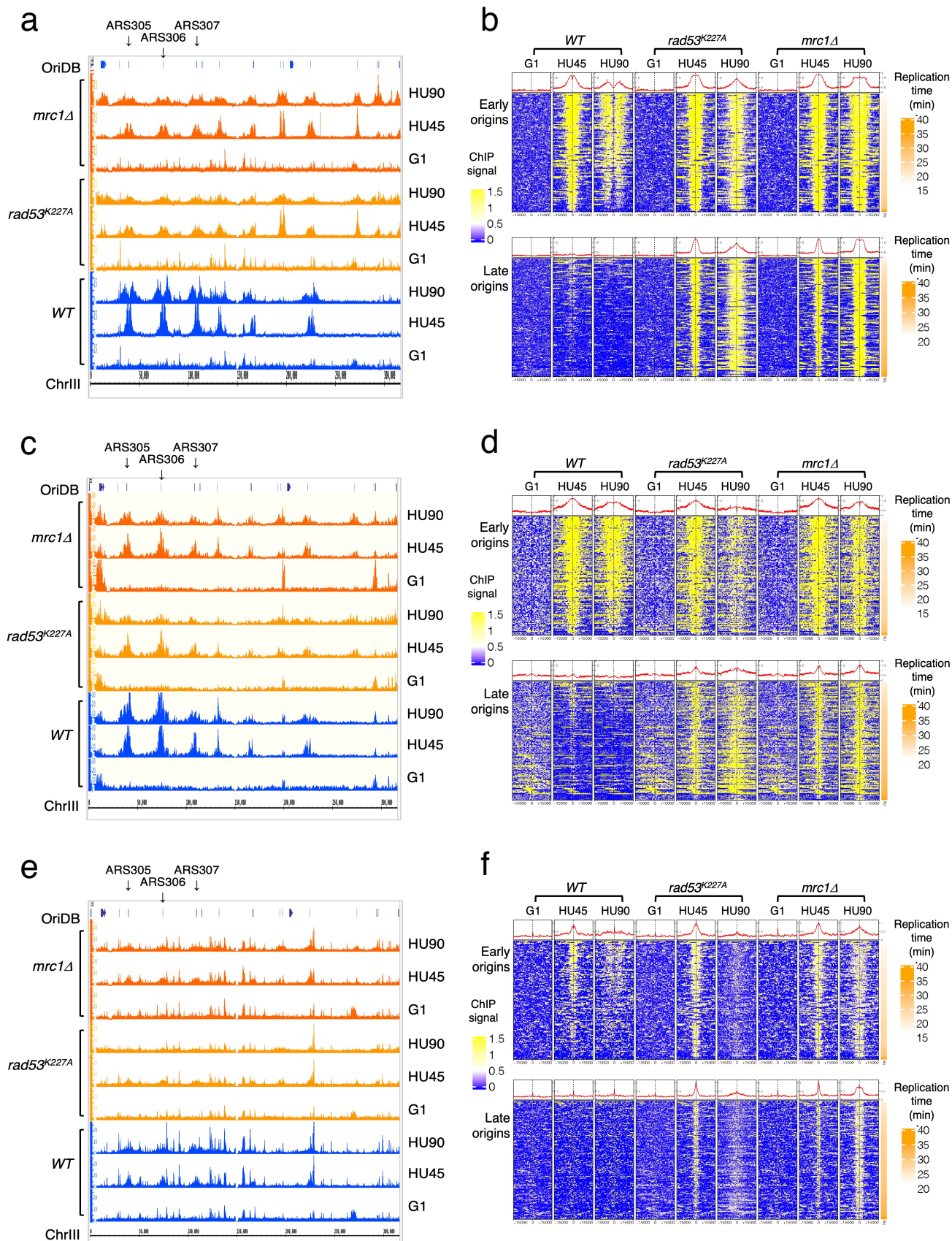


Figure 2 – figure supplement 1

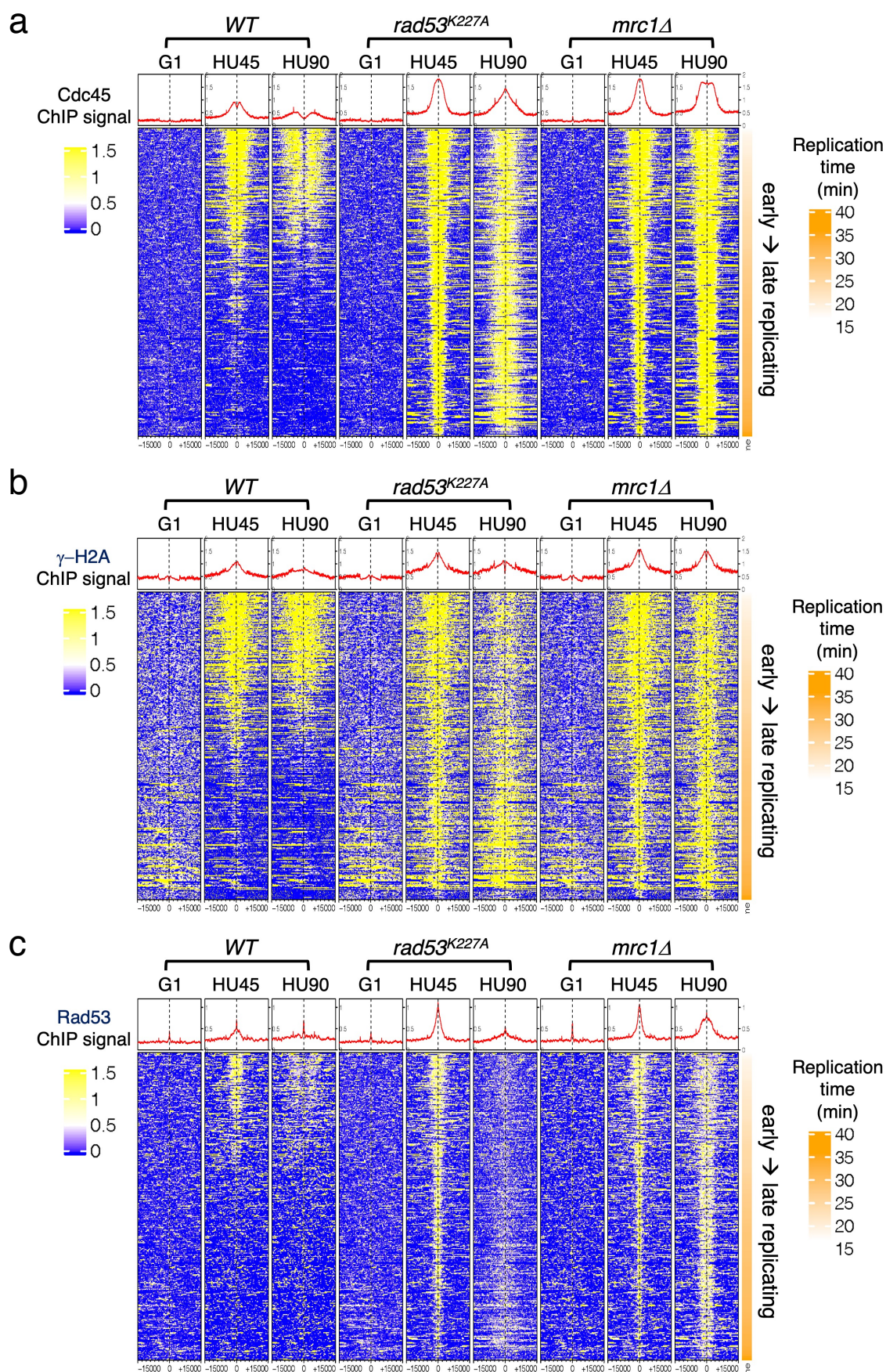


Figure 3

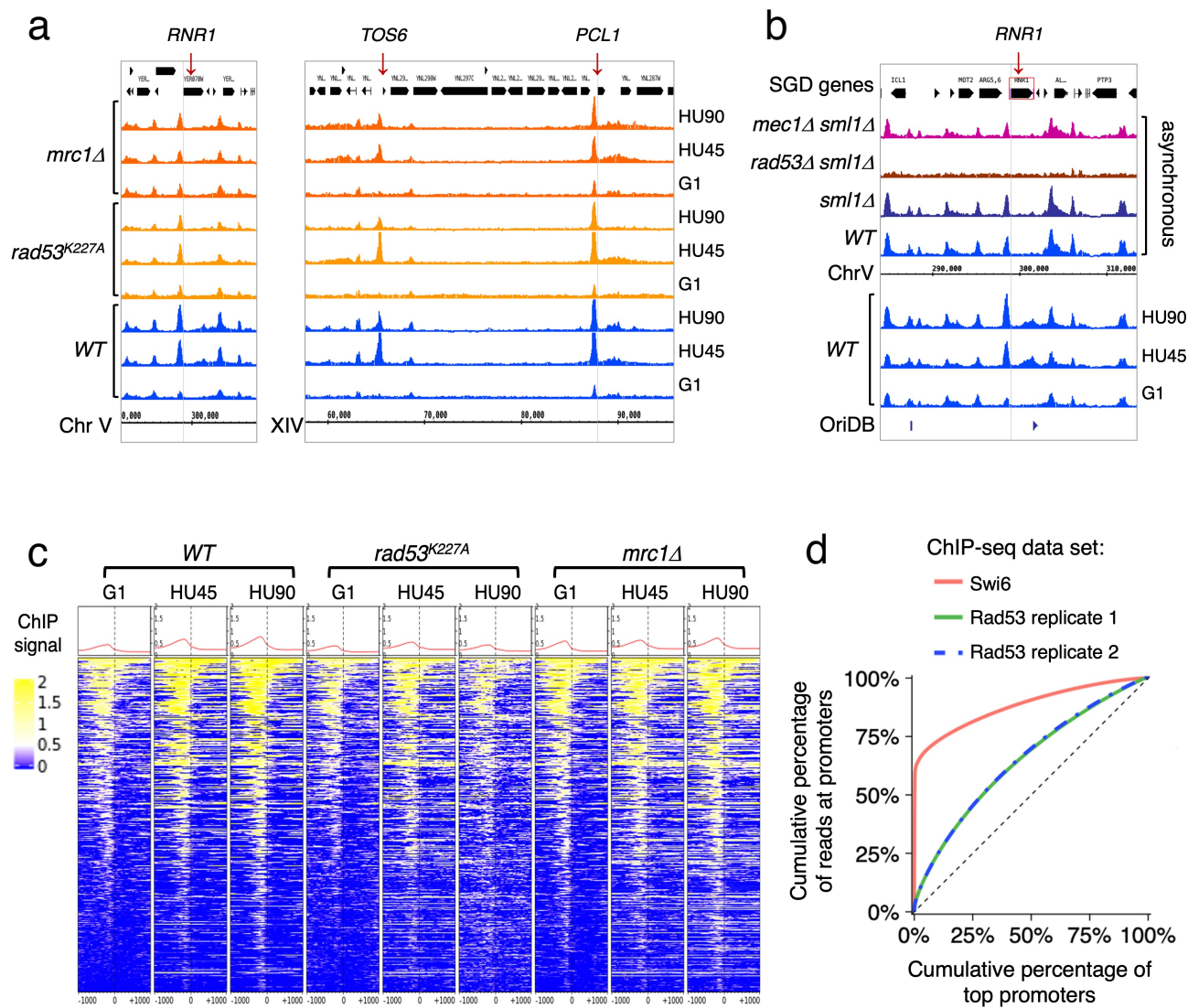
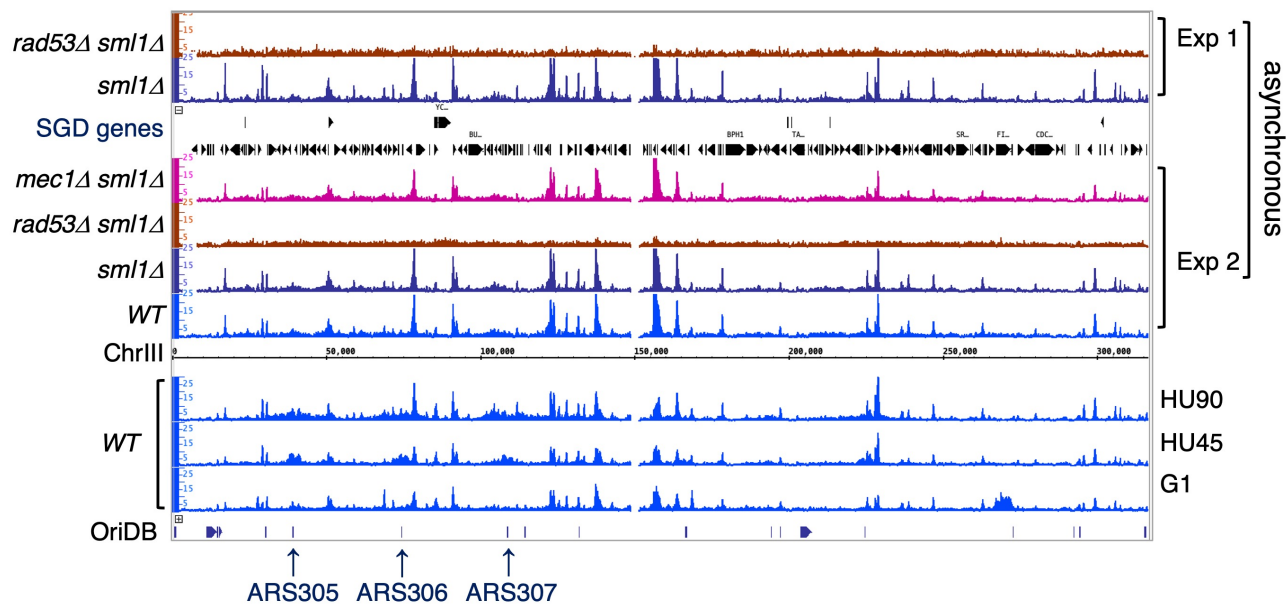


Figure 3 – figure supplement 1

a

Rad53 ChIP-seq in WT and mutant cells



b

Distribution of Rad53 peaks in relation to genes

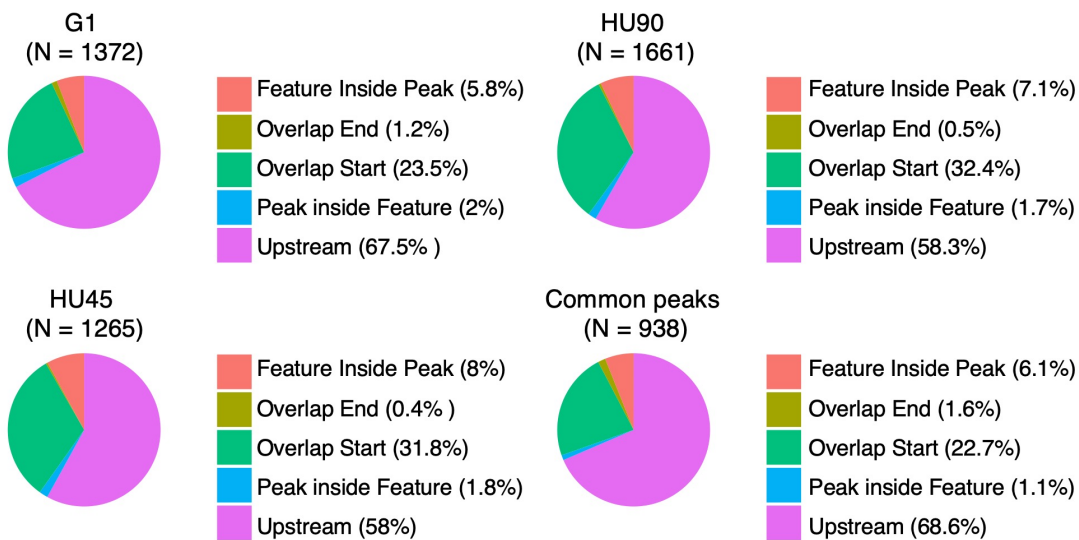


Figure 3 – figure supplement 2

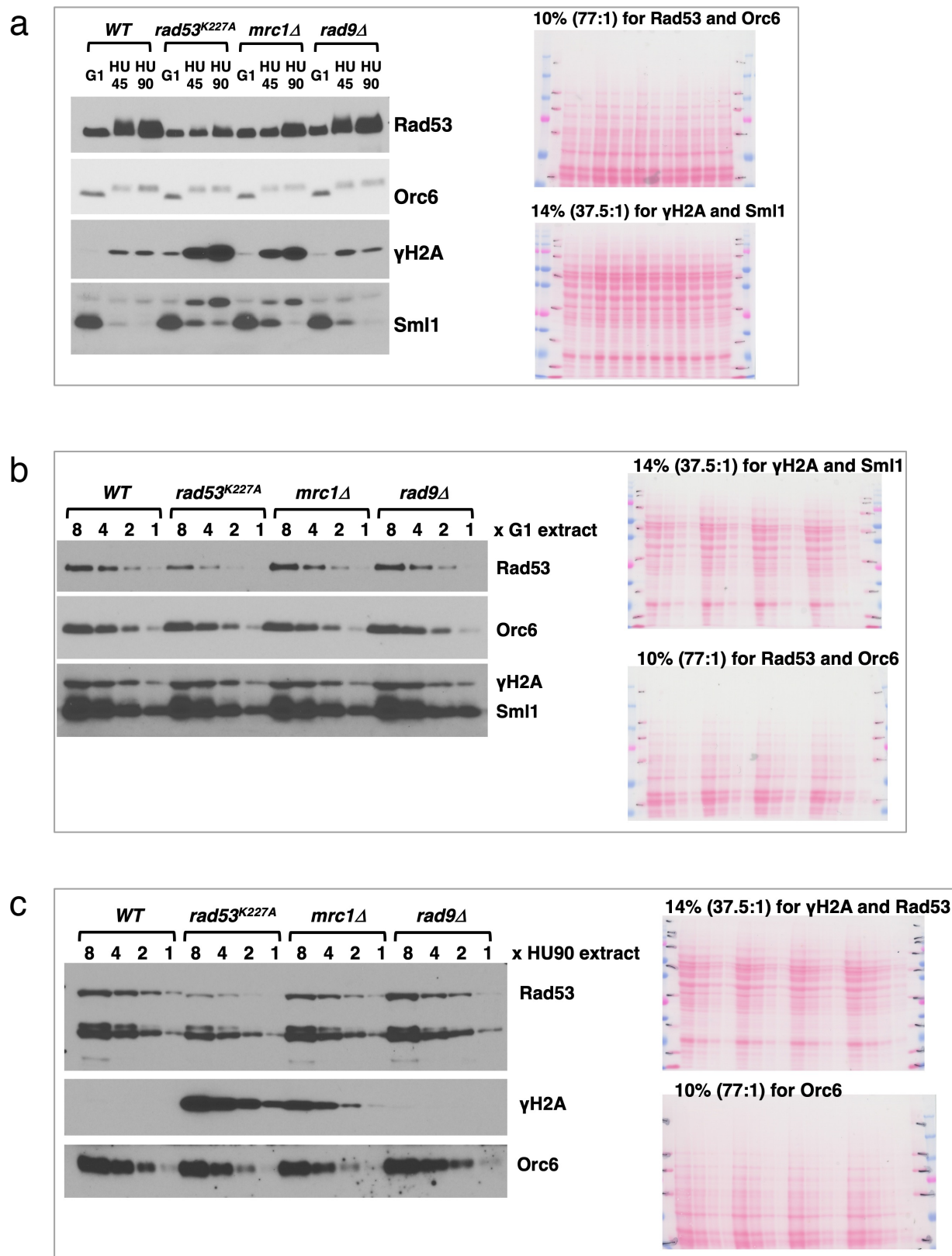
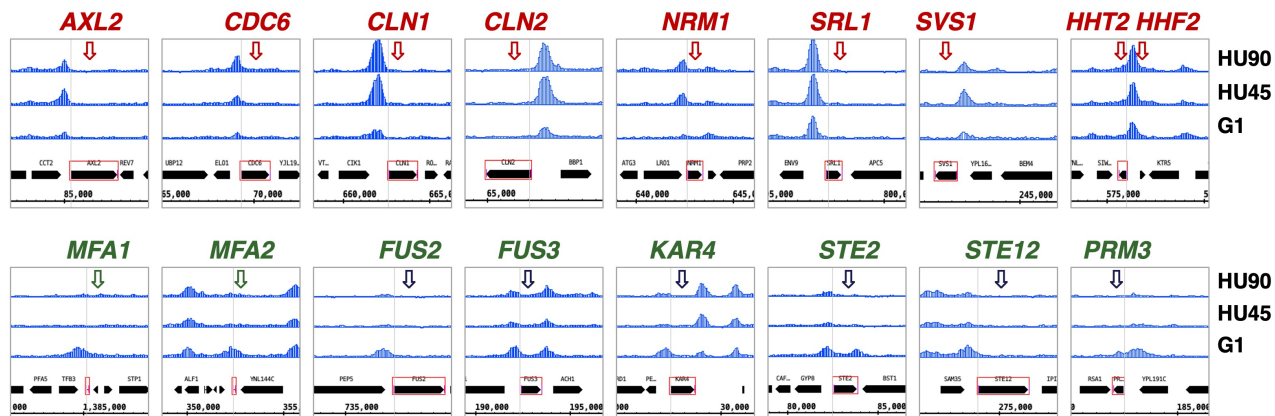
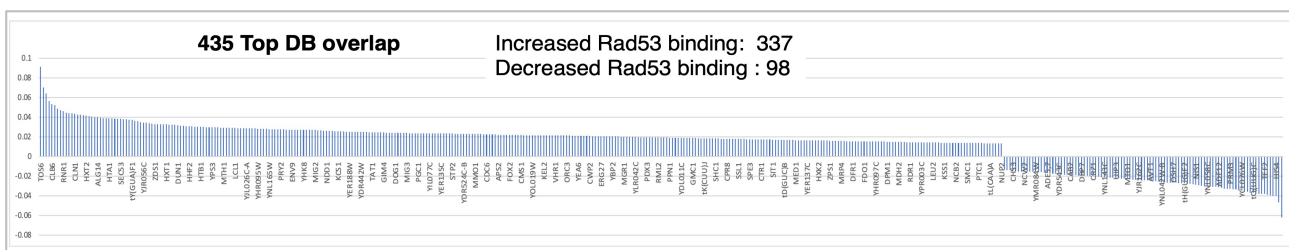


Figure 4

a



b



c

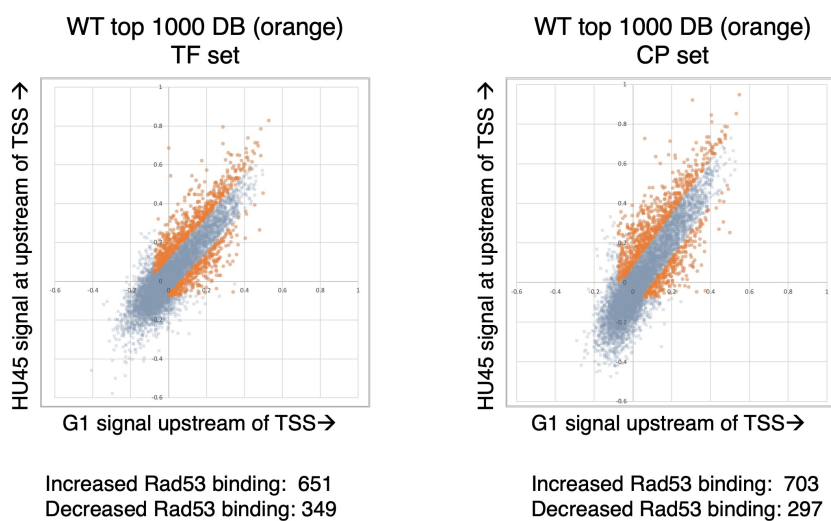


Figure 5

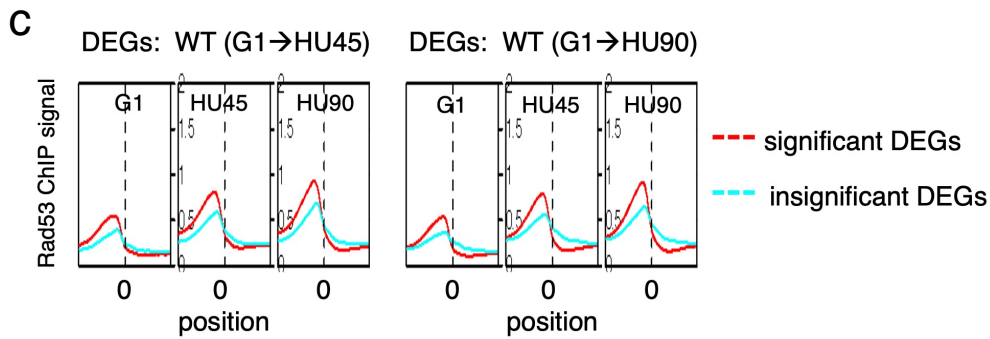
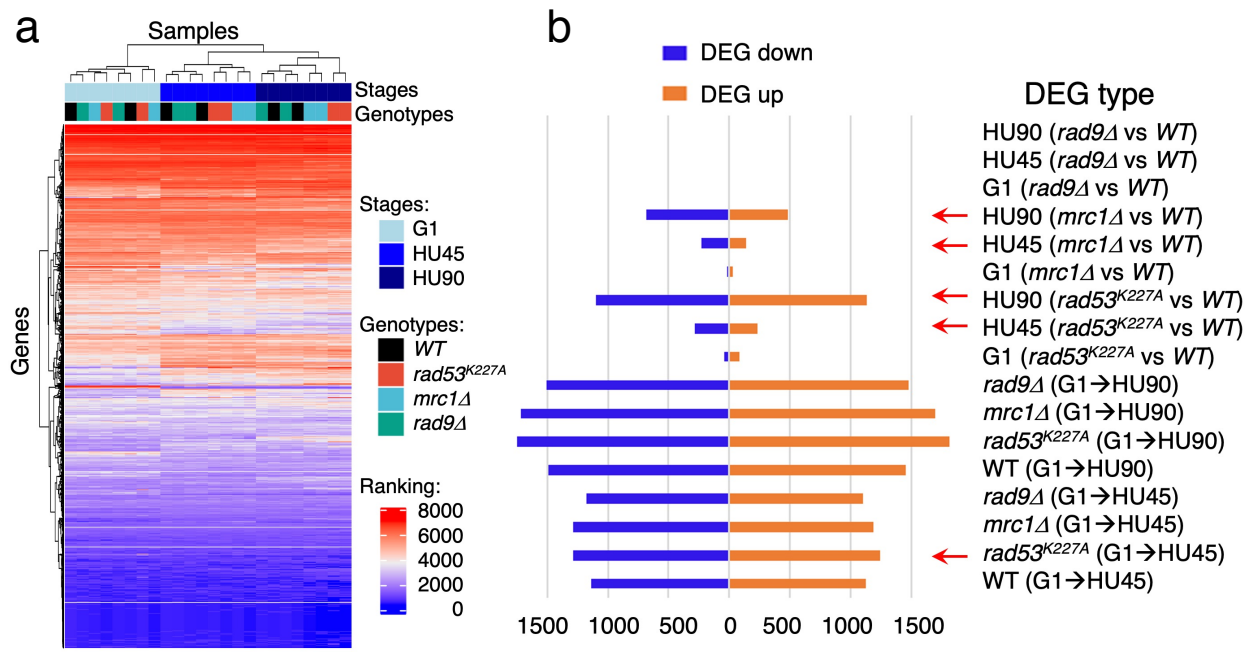


Figure 5 – figure supplement 1

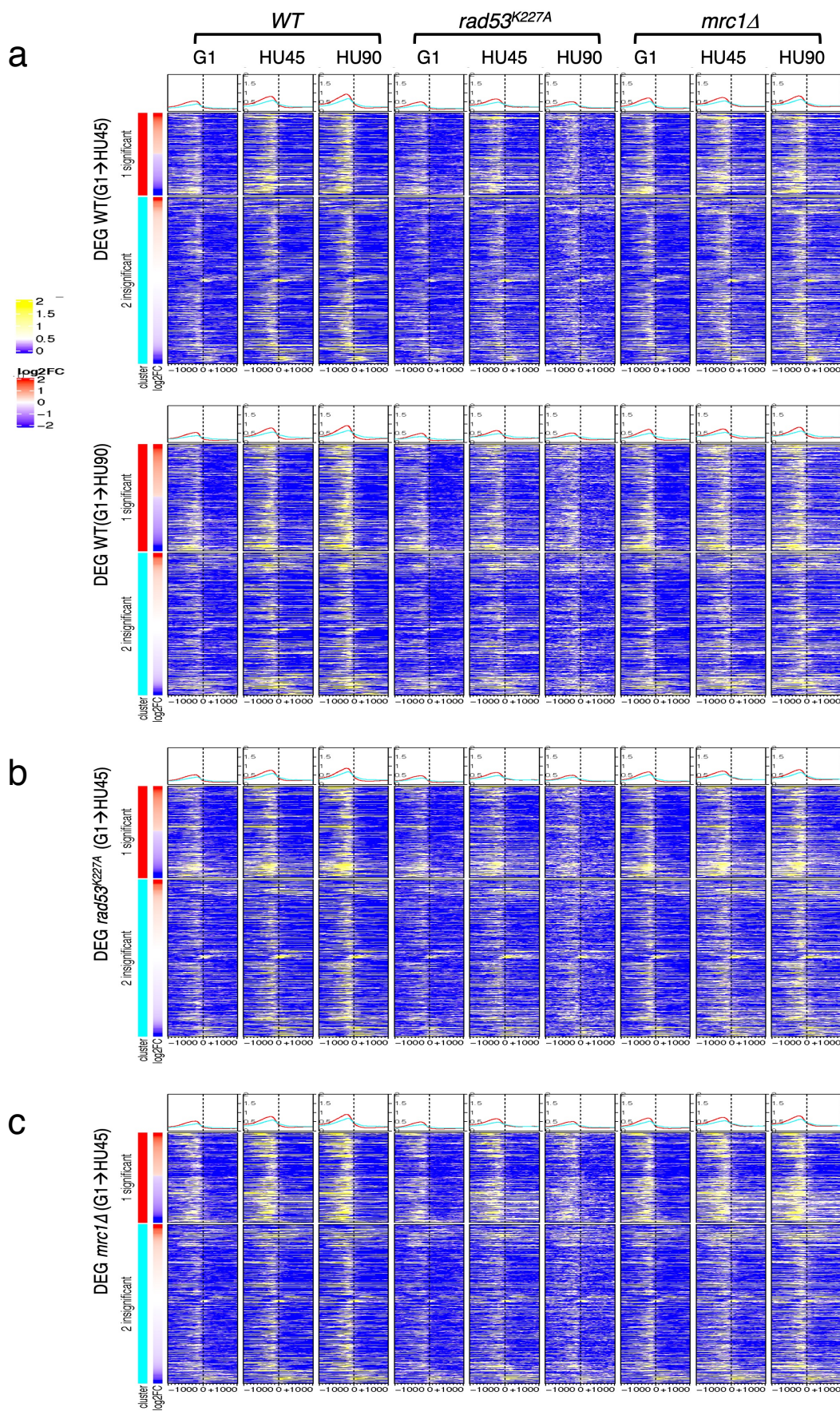


Figure 6

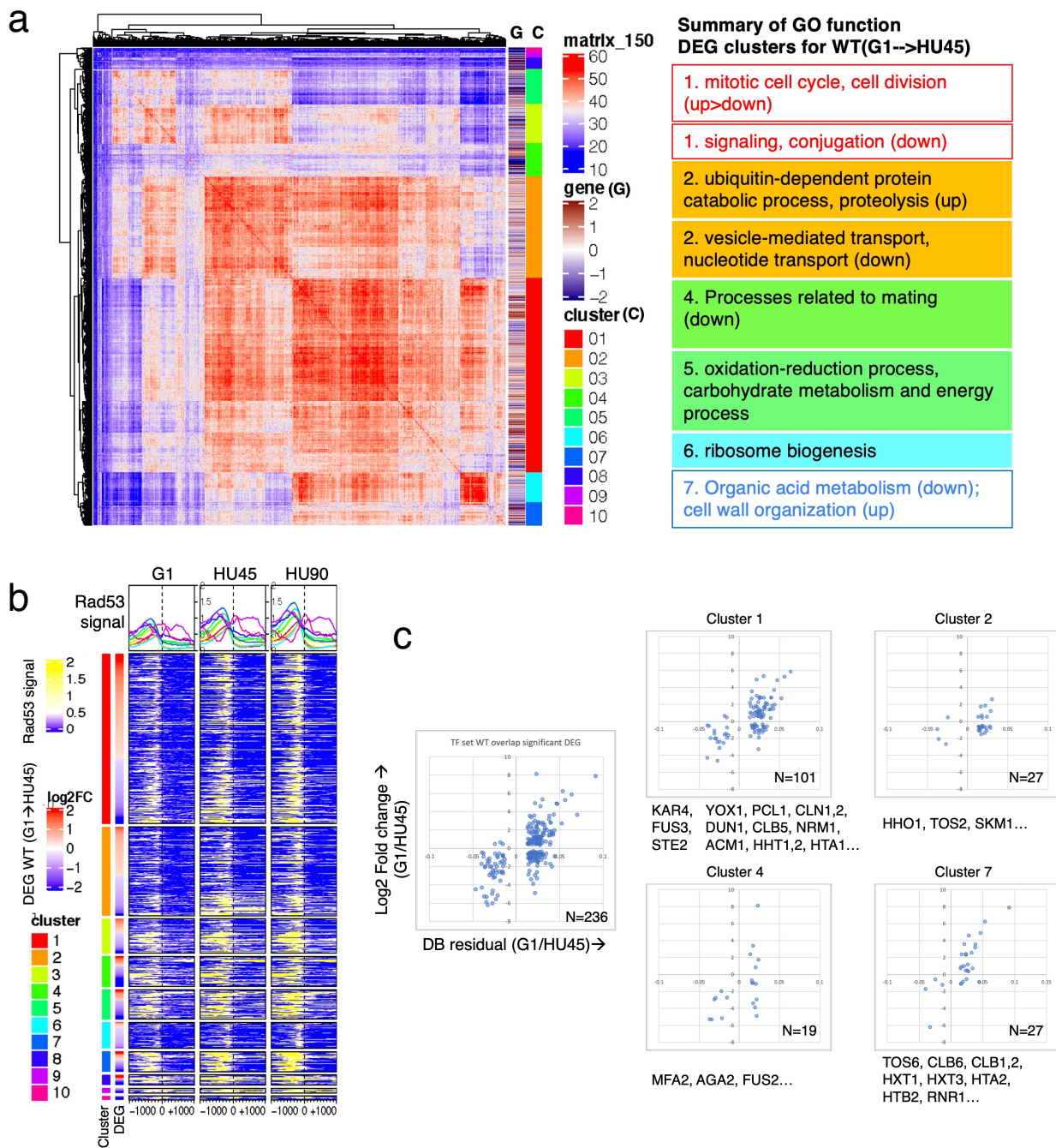


Figure 6 – figure supplement 1

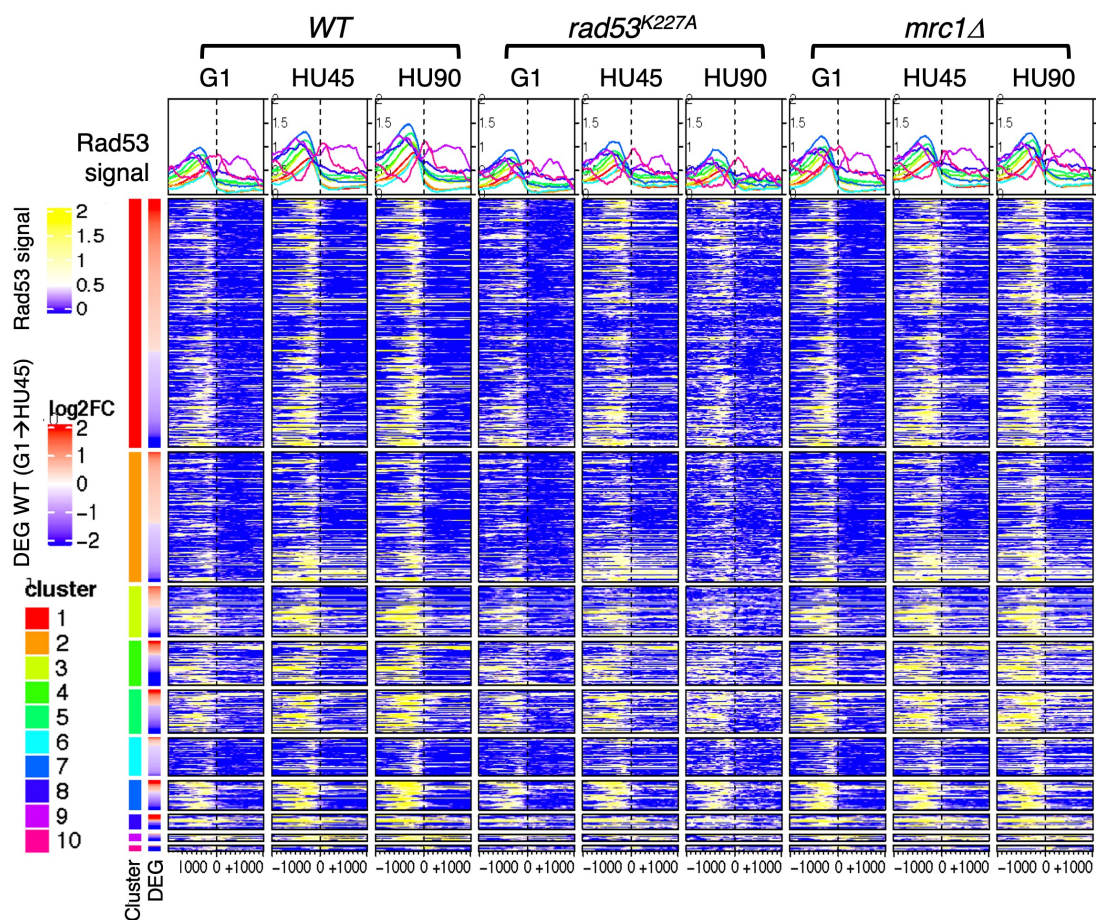


Figure 7

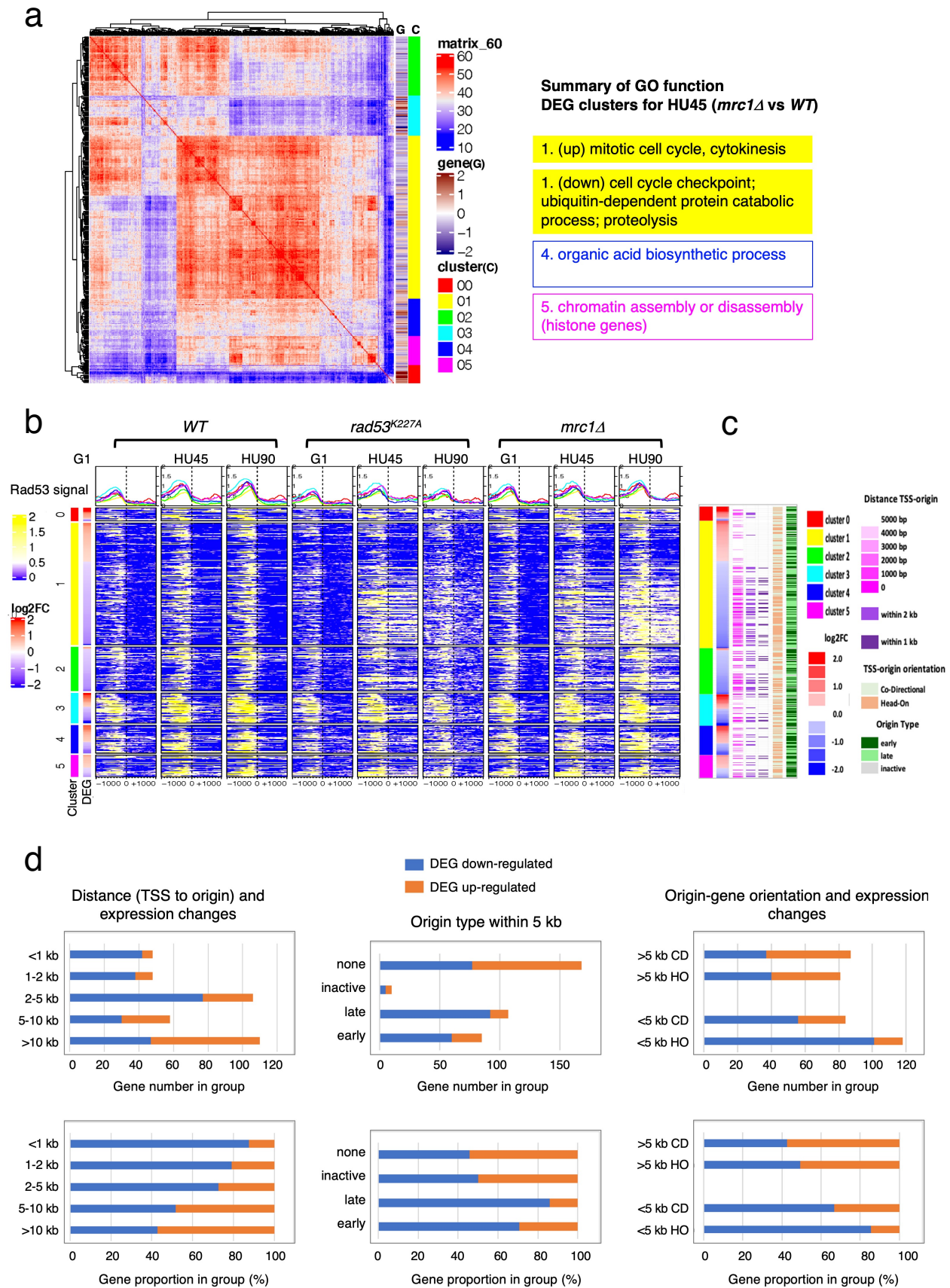


Figure 7 – figure supplement 1

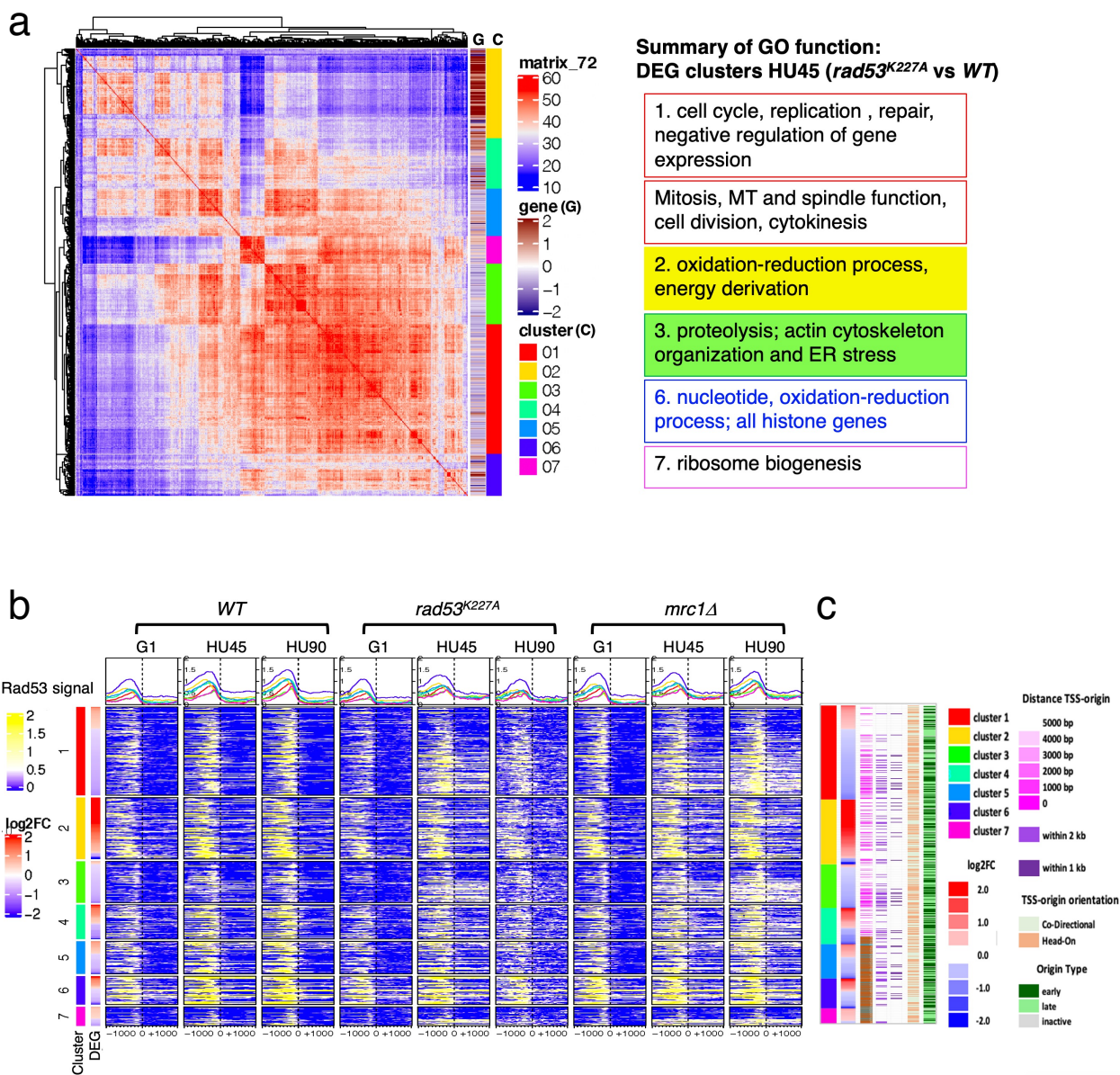


Figure 8

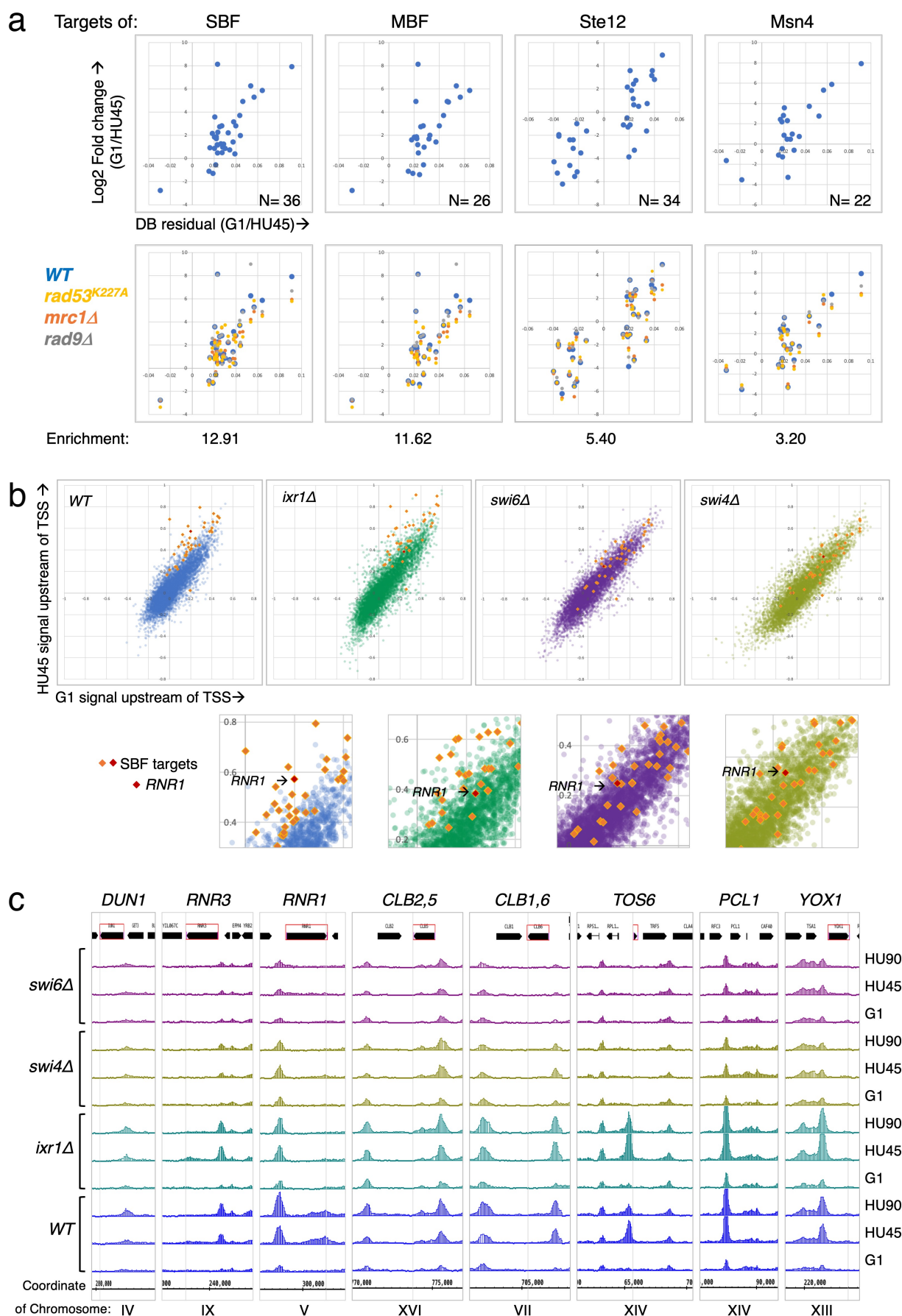


Figure 8 – figure supplement 1

